Fail-safe optimization of tubular frame structures under stress and eigenfrequency requirements

Dou, Suguang; Stolpe, Mathias

Published in:
Computers & Structures

Link to article, DOI:
10.1016/j.compstruc.2021.106684

Publication date:
2022

Document Version
Peer reviewed version

This manuscript has been reviewed and accepted for publication in the journal of Computers and Structures on 24 September 2021

Fail-safe optimization of tubular frame structures under stress and eigenfrequency requirements*

Suguang Dou† and Mathias Stolpe‡

September 27, 2021

Abstract

In conventional fail-safe optimization of frame structures the damage is usually modelled as complete removal of one or more members. We propose and incorporate two additional types of damage models into the fail-safe design problem. The first describes thickness degradation caused e.g. by corrosion. The second describes severe local damage by removal of a part of a member that causes a gap and free ends in the member. The latter damage model can cause undesirable local vibration modes. By combining the two damage models, local thickness degradation in a part of a member can be modelled. The considered design problem minimizes structural mass and includes local stress constraints and limits on eigenfrequencies. Besides the new damage models, a working-set algorithm is applied on the fail-safe optimization problem to reduce the computational cost. Numerical experiments on two-dimensional frame structures illustrate that the working-set algorithm can effectively handle the relatively large number of constraints and damage scenarios in fail-safe optimization.

Keywords: Fail-safe structural optimization, local stress constraints, tubular frame structure, eigenfrequency constraints, working-set algorithm

1 Introduction

We propose problem formulations for fail-safe sizing optimization of tubular frame structures subjected to static loads that extend current capabilities in the field. The problems include local static stress constraints and eigenfrequency limits and are, in that respect, similar to the problems studied already in the 1970s in [44] and the 1980s in [7]. In [44] and [7] minimum weight truss sizing problems with constraints on local stresses, nodal displacements, eigenfrequencies and buckling load constraints are

*The research is funded by the Independent Research Fund Denmark through the research project *Fail-Safe Structural Optimization* (SELMA) with grant no. 7017-00084B.

†Technical University of Denmark (DTU), DTU Wind Energy, Fredriksborgvej 399, 4000 Roskilde, Denmark. E-mail: sudou@dtu.dk

‡Technical University of Denmark (DTU), DTU Wind Energy, Fredriksborgvej 399, 4000 Roskilde, Denmark. E-mail: matst@dtu.dk, Phone: (+45) 2151 8240

presented. The problems proposed in [44] and [7] are in some sense more complicated than the problems studied herein. We ignore buckling and nodal displacement constraints and use a different structural analysis model. The damage scenarios used in [44] model complete removal of one member. In [7] complete removal of a group of members is modelled. The damage models are here extended to additionally include local thickness degradation, loss of parts of members, and loss of several members.

Fail-safe structural optimization is important when it is required that the structure can function safely even with members missing or at reduced capacity, i.e. when it is required that the structure can resist the given loads even when a load path vanishes. The analyses in fail-safe optimization are generally restricted to linear static analyses rather than more advanced nonlinear static and dynamic analyses such as those used in the related studies of progressive collapse multi-story buildings [22, 49]. This may be attributed to the computational complexity of fail-safe optimization itself and thus fast analyses which additionally allow for analytical design sensitivity analysis are preferred. It is noted in [29] that optimizing lattice structures without fail-safe requirements will not, in general, lead to fail-safe designs. Similar observations are also made in e.g. [44] and [7]. The importance of fail-safe or redundancy structural optimization has resulted in several research articles over the past decades. Optimal structural design with degradation is covered in e.g. [10] and [4]. Models for redundancy optimization of (truss) structures is the topic of several articles including [45], [9], [25], [30], and [24]. Models and algorithms for fail-safe topology optimization through density based approaches and material interpolation schemes are presented in e.g. [23], [51], [33], [28], [19], [15], [6], [40], and [50]. Fail-safe optimal design in the framework of fracture mechanics and uncertainty analysis is studied in [39]. Recently fail-safe optimization of beam structures has been studied in [29]. The problems considered in [29] are minimum mass problems with several local stress constraints per member and damage scenarios involving the loss of some members in the frame. Several heuristic approaches to reduce the computational demands are presented and assessed. The stress constraints in [29] are aggregated using a p-norm. We instead include the constraints without aggregation and associated approximation.

We consider fail-safe structural optimization while including important performance measures, notably stresses and frequency limits. Stress constraints in structural optimization has been a topic of study since the 1960s. Many of the studies address the stress-singularity problem (also known as singular optima, singular optimal topologies) which is especially well studied for truss topology optimization problems in e.g. [46], [38], [26, 27], [35, 36] and [12]. The issue occurs for topology optimization problems with stress constraint, in that the local stress constraints should be removed if the corresponding design variable becomes zero, i.e. if a member vanishes. With reasonable modelling of the variable bounds, stress-singularity should not be an issue for sizing optimization of e.g. trusses and frame structures. For sizing problem, the local stress constraints should not be removed due to the current values of the design variables. However, when considering certain damage scenarios in fail-safe structural optimization, mechanisms similar to stress-singularity become an issue which can create non-intuitive results. The brief note [18] studies the influence of the modelling of the local stress constraints by analytically solving a small-scale truss sizing problem instance. We propose capabilities to include thickness degradation and model the local stress

constraints differently than in [44] and [29]. Fail-safe structural optimization problems with local stress constraints generally lead to nonlinear optimization problems with potentially many constraints and a dense and computationally expensive Jacobian of the constraints. We therefore tailor a recently proposed working-set approach to handle this aspect of fail-safe sizing optimization of tubular frame structures. The working-set approach is based on the one suggested in [48] for frame-optimization problems under transient loads and local stress constraints, and in [41] for fail-safe truss topology optimization. A similar technique is used in [34] for fail-safe optimization of fluid viscous dampers for seismic retrofitting of frame structures. Several working-set approaches have been suggested in the structural optimization community, especially for topology optimization problems with local stress constraints. Two examples of approaches where constraints are allowed to enter and leave the working-set for this particular type of problems are proposed in [20] and [11]. The working-set approach adopted herein differs from these approaches since a sequence of sub-problems, each with a fixed set of constraint, is solved. The type of proposed working-set approach, as also mentioned in [48] and [41], can be applied to problems with a very large number of nonlinear constraints but with a modest number of design variables. In this situation, it is possible, but by no means guaranteed, that the number of active constraints at the optimum is relatively low.

The motivation for this work is the future extension of the capabilities for design optimization of offshore wind turbine support structures such as jackets. These are often modelled and constructed as welded assemblies of steel members with circular and hollow cross-sections. Several articles cover structural optimization of wind turbine support structure optimization, see e.g. [31], [13], [37], and [32] among others. The aim of the present work is to lay the foundations for this application by proposing and studying relevant problem formulations and assessing an optimization algorithm through reproducible numerical examples. Offshore support structures should preferably be designed with responses from coupled aero-hydro-servo-elastic simulations which makes replication of the results more difficult. This particular kind of application is therefore considered future work,

This manuscript is organized in the following manner. First comes a brief overview of the structural analysis models, a unified formulation of several different degradation and damage models, and the couplings between the structural analysis and the damages models through the finite element stiffness and mass matrices. This is followed by statements of the optimal design problems, one for nominal design and two different problems for fail-safe design. The first fail-safe problem considers partial degradation of the thickness of (parts of) members where as the other considers complete removal of one or several (parts of) members. The next topic is a presentation of the working-set algorithm and the implementation of the structural analysis routines and the optimization algorithm. The algorithm is used to produce the numerical results that are based on sizing optimization of three 2D tubular frame structures subjected to different loading scenarios and with different numbers of members. Several different types of damage scenarios and different degradation levels are investigated. The optimal designs and the corresponding worst-case damage scenarios are presented. The behaviour of the optimal objective value is studied for one example, as the level of partial degradation is increased from zero to almost complete loss of a member. The results are followed

by a general discussion covering the limitations of the models and algorithms. Finally, the manuscript contains a list of the main conclusions.

2 Fail-safe optimal design problem

For frame structure optimization several design variables are normally associated with a member, since several parameters are generally required to describe beam cross-sections. In the numerical experiments, we focus on hollow thin-walled circular cross-sections. The cross-sections of the beams are described by two variables, the outer diameter d_i and the material thickness t_i of the ith beam member in the frame structure. This is an arbitrary choice of cross-section but it is motivated by the intended future application of optimal design of offshore support structures for wind turbines. The way of describing the cross-section is non-unique and it is chosen because it is common for the considered application, see e.g. [32] and [37]. In any case, the mathematical notation is almost general and generalizations to other cross-section geometries is often straightforward. In the modelling and the numerical computations, we collect the design variables associated with a specific beam element in the vector $\mathbf{v}_e$. In our case, $\mathbf{v}_e = \begin{pmatrix} d_e & t_e \end{pmatrix}^T$. These are in turn collected into the vector $\mathbf{v} = \begin{pmatrix} \mathbf{v}_1^T & \mathbf{v}_2^T & \cdots & \mathbf{v}_{n_e}^T \end{pmatrix}^T$, where n_e is the number of elements in the undamaged ground structure. Note that variable linking or grouping are used in the optimization such that the elements in the same member are assigned the same design variables. It should be mentioned that not all variables associated with a beam need to be included in the damage scenarios. In our examples only the thickness is directly included in the damage model. The outer diameter is changed as a consequence. If another design description is used, e.g. with thickness and inner diameter as design variables, the modelling becomes slightly different.

2.1 Frame analysis and design sensitivity analysis

The frame analysis is based on the finite element method under the assumptions of linear elasticity and Euler-Bernoulli beam theory. Details of the used beam element and the mesh are given in the numerical experiments section. The nominal static equilibrium equations, i.e. the equations for the undamaged structure, are $\mathbf{K}(\mathbf{v})\mathbf{u} = \mathbf{f}$, where $\mathbf{K}(\mathbf{v})$ is the nominal stiffness matrix, $\mathbf{u}$ contains the nodal displacements and rotations, and the external load vector $\mathbf{f}$ is assumed to be design-independent. Extensions to design-dependent loads, e.g. self-weight, are possible after modifications of the design sensitivity analysis. The static equilibrium equations for damage scenario j are $\mathbf{K}^{(j)}(\mathbf{v})\mathbf{u}^{(j)} = \mathbf{f}$. The eigenvalue problem for the nominal, i.e. undamaged, design $\mathbf{v}$ is

$$(\mathbf{K}(\mathbf{v}) - \lambda_k \mathbf{M}(\mathbf{v}))\boldsymbol{\theta}_k = \mathbf{0}, \tag{1}$$

where $\mathbf{M}(\mathbf{v})$ is the nominal mass matrix for the frame. The eigenvalues are assumed to be ordered $0 \leq \lambda_1 \leq \lambda_2 \leq \cdots$. The eigenvalue problem for damage scenario j is

similarly defined by

$$(\mathbf{K}^{(j)}(\mathbf{v}) - \lambda_k^{(j)}\mathbf{M}^{(j)}(\mathbf{v}))\boldsymbol{\theta}_k^{(j)} = \mathbf{0}. \tag{2}$$

The eigenfrequencies in Hz are calculated as $f_k = \sqrt{\lambda_k}/(2\pi)$, and used in the numerical implementation.

With the choice of cross-section geometry and the definition of the design variables it is possible to provide analytical expressions for the partial derivatives of mass and stiffness matrices with respect to the design variables. With this information it is straightforward to compute design sensitivities of the displacement vector with respect to some design variable v. Here it is assumed that the displacement vector satisfies the static equilibrium equations. Using standard results from e.g. [14] we obtain

$$\frac{\partial \mathbf{u}^{(j)}(\mathbf{v})}{\partial v} = -\left(\mathbf{K}^{(j)}(\mathbf{v})\right)^{-1} \frac{\partial \mathbf{K}^{(j)}(\mathbf{v})}{\partial v}\mathbf{u}^{(j)}(\mathbf{v}). \tag{3}$$

Based on (3), direct differentiation is used in the design sensitivity analysis of the local stress constraints. The derivatives of local stress with respect to the element-wise displacements can be seen in [29]. In case of complete removal of (parts of) members, the stresses in the removed (parts of) members are not evaluated. The following subsection introduces the damage models and the stiffness and mass matrices for the damaged (parts of) members.

Under the (possibly unrealistic) assumption that the eigenfrequencies do not coincide and causing issues with non-differentiability [14], the following design sensitivity is used for the eigenvalues

$$\frac{\partial \lambda_k^{(j)}}{\partial v} = -(\boldsymbol{\theta}_k^{(j)})^T \left(\frac{\partial \mathbf{K}^{(j)}(\mathbf{v})}{\partial v} - \lambda_k^{(j)}\frac{\partial \mathbf{M}^{(j)}(\mathbf{v})}{\partial v}\right)\boldsymbol{\theta}_k^{(j)}. \tag{4}$$

The sensitivity of the eigenfrequency is calculated as $\frac{\partial f_k^{(j)}}{\partial v} = \frac{1}{2\pi\sqrt{\lambda_k^{(j)}}}\frac{\partial \lambda_k^{(j)}}{\partial v}$.

2.2 Damage models

This section gives a description of the considered damage models with an increasing level of modelling capabilities. Existing studies of fail-safe optimization are mostly based on complete loss of an entire member, see e.g. [29]. A few studies examined the scenarios of partial damage of an entire member [44, 41]. No research has, as far as the authors are aware, studied partial damage or complete loss of a part of a member in combination with optimal design. This study provides a unified formulation of the damage model to describe the level of damage (e.g. degradation or complete loss), as well as the spatial distribution of the damage (e.g. an entire member or a part of a member), and extend the damage models for solid beams to tubular beams. We note that the presented damage models neither consider damage initiation or propagation, nor progressive failures. The models also assume linear elasticity, also in the damaged situation. The two representative damage models that we consider for beams with tubular cross-sections are illustrated in Figure 1. This figure 1 also shows the definition

of member/part/element and four different damage scenarios. One member is seen as a body of 4 parts with equal length. When the damage occurs on the level of part, one arbitrary part can be removed.

Let the parameter $\gamma \in [0,1]$, i.e. the relative degradation, describe the extent of the damage, and $\gamma_e^{(j)} \in [0,1]$ describe the damage level of the eth element in scenario j. The damage models are essentially based on thickness degradation to the point that the material has zero thickness. For the choice of hollow circular cross-sections, the thickness after degradation becomes $t_e^{(j)} = t_e\,(1-\gamma_e^{(j)})$ for $\gamma_e^{(j)} \in [0,1]$. The degradation additionally results in a reduction of the outer diameter of the cross-section through $d_e^{(j)} = d_e - 2\,\gamma_e^{(j)}\,t_e$. For all elements, their outer diameters and thicknesses can be written in a unified form as

$$\mathbf{v}_e^{(j)} = \begin{pmatrix} d_e - 2\,\gamma_e^{(j)}\,t_e \\ t_e\,(1-\gamma_e^{(j)}) \end{pmatrix}. \tag{5}$$

where $\gamma_e^{(j)} = 0$ for undamaged elements, and $\gamma_e^{(j)} = \gamma$ for damaged elements.

The set of damaged elements vary with the damage scenario. Let the index-set $\mathcal{D}_j \subseteq \mathcal{E}$ denotes the (sub-)set of damaged elements which are involved in the scenario j, and the corresponding set of undamaged elements is denoted as $\mathcal{E} \setminus \mathcal{D}_j$. The element-wise damage level for scenario j is thus given as

$$\gamma_e^{(j)} = \begin{cases} 0 & \text{if } e \in \mathcal{E} \setminus \mathcal{D}_j \\ \gamma & \text{if } e \in \mathcal{D}_j \end{cases} \tag{6}$$

As a result, the stiffness and mass matrices for an arbitrary scenario j can also be written in a unified form as

$$\mathbf{K}^{(j)}(\mathbf{v}) = \sum_{e\in\mathcal{E}} \mathbf{K}_e\left(\mathbf{v}_e^{(j)}\right), \quad \mathbf{M}^{(j)}(\mathbf{v}) = \sum_{e\in\mathcal{E}} \mathbf{M}_e\left(\mathbf{v}_e^{(j)}\right). \tag{7}$$

where $\mathbf{K}_e$ and $\mathbf{M}_e$ are the e^{th} element's stiffness and mass matrices calculated based on $\mathbf{v}_e^{(j)}$.

2.3 Problem statements

In the nominal design problem, no degradation or damages are modelled, i.e. the nominal problem is a classical frame sizing problem with mass as the objective and limits on stresses and eigenfrequencies. The eigenfrequency constraints are motivated by the intended application in wind energy, namely optimization of support structures for wind turbines. The frequency constraints are intended to ensure that the system frequencies remain sufficiently far away from the first few operating frequecies of the wind turbine. The nominal minimum mass problem that we consider is

$$\begin{array}{lll} \underset{\mathbf{v}\in\mathcal{F}}{\text{minimize}} & m(\mathbf{v}) & \\ \text{subject to} & \underline{\boldsymbol{\sigma}} \le \boldsymbol{\sigma}_e(\mathbf{v}) \le \overline{\boldsymbol{\sigma}} & \forall\, e \in \mathcal{E}, \\ & \underline{f}_k \le f_k(\mathbf{v}) \le \overline{f}_k & \forall\, k = 1,\ldots,p, \end{array} \tag{P_N}$$

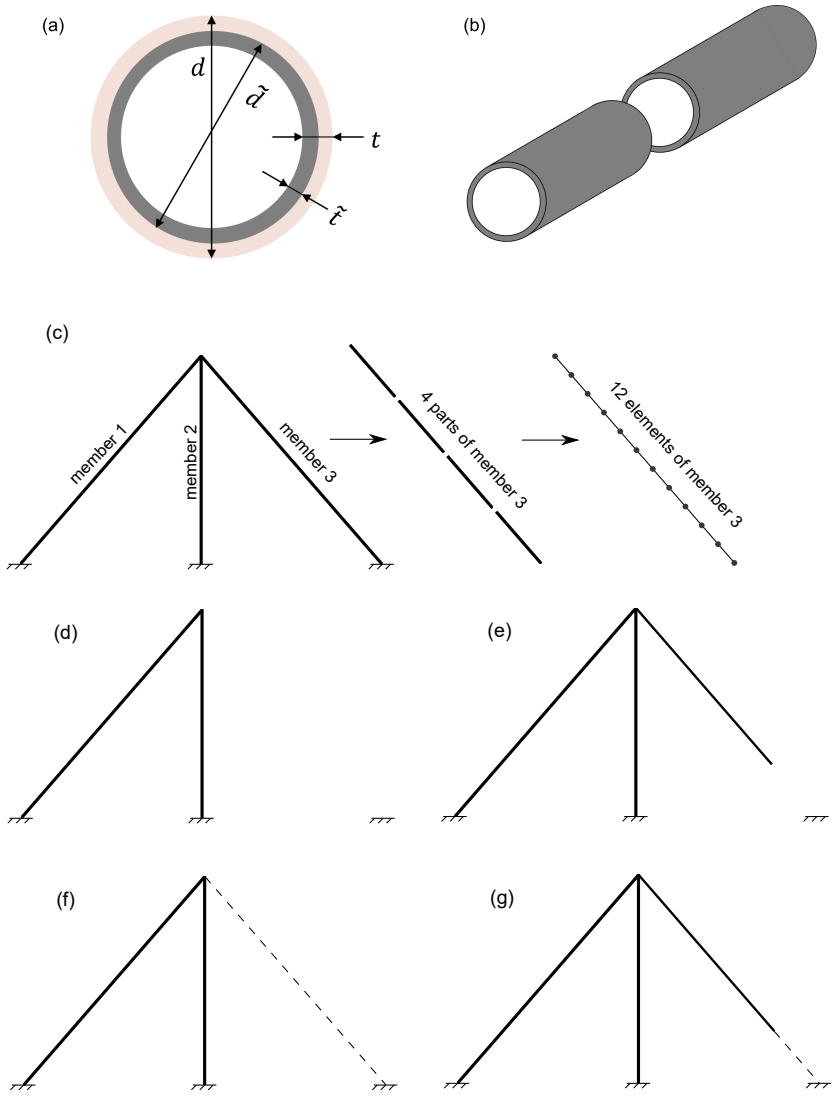

Figure 1: Illustration of damage models, definition of member/part/element, and damage scenarios. (a) Thickness degradation of tubular cross-section. (b) Complete loss of one part of a member. (c) The configuration of members, parts and elements. (d) Damage scenario of complete loss of member 3. (e) Damage scenario of complete loss of one part of member 3, resulting in a beam with a free end. (f) Thickness degradation of the entire member 3. (g) Thickness degradation of one part of member 3. In (f) and (g) the dash line represents the spatial location of the thickness degradation.

where $\boldsymbol{\sigma}_e$ represents stresses evaluated at specific points in finite element e. The stress limits are provided in $\underline{\boldsymbol{\sigma}}$ and $\overline{\boldsymbol{\sigma}}$ with $\underline{\boldsymbol{\sigma}} \leq \overline{\boldsymbol{\sigma}}$. Similarly, the lower and upper limits on the kth eigenfrequency are provided in $\underline{f}_k$ and $\overline{f}_k$ with $\underline{f}_k \leq \overline{f}_k$ for all k. The set $\mathcal{F}$ models the bounds on the variables and any general linear constraints, i.e.

$$\mathcal{F} = \{\mathbf{v} \mid \underline{\mathbf{v}} \leq \mathbf{v} \leq \overline{\mathbf{v}}, \mathbf{A}\mathbf{v} \leq \mathbf{b}\},$$

where $0 \leq \underline{v}_j \leq \overline{v}_j < +\infty$ for all j are the bounds on the design variables. The user supplied matrix $\mathbf{A}$ and the vector $\mathbf{b}$ are of suitable dimensions. The linear constraints $\mathbf{A}\mathbf{v} \leq \mathbf{b}$ are used to model the requirements on the minimum and maximum ratios of diameter to thickness in the numerical examples. It is assumed that the set $\mathcal{F}$ is non-empty. Problem P_N thus contains local stress constraints in all members and all finite elements in the frame. This can be modified e.g. by replacing the set $\mathcal{N}$ with another set. Note that problem P_N is stated as a single load problem in order to avoid complicating the notation more than necessary. Extensions to multiple loads are of course possible by including stress constraints for each load case.

There are several ways to model a fail-safe problem corresponding to P_N. The choice depends on e.g. the properties of the damage scenarios. For problems with only degradation, i.e. no part or member vanishes in the damage scenario, we require that all local stress constraints remain in the problem. Based on the analytical results on a small-scale truss example in the brief note [18], this decision can cause the objective function to increase significantly with increases in the damage parameter γ. A fail-safe variant of the nominal problem P_N with only degradation is

$$\begin{aligned} \underset{\mathbf{v}\in\mathcal{F}}{\text{minimize}} \quad & m(\mathbf{v}) \\ \text{subject to} \quad & \underline{\boldsymbol{\sigma}} \leq \boldsymbol{\sigma}_e^{(j)}(\mathbf{v}) \leq \overline{\boldsymbol{\sigma}} \qquad \forall\, j \quad \forall\, e \in \mathcal{E}, \\ & \underline{f}_k^{(j)} \leq f_k^{(j)}(\mathbf{v}) \leq \overline{f}_k^{(j)} \quad \forall\, j \quad \forall\, k = 1, \ldots, p. \end{aligned} \tag{$P^{\gamma\in(0,1)}$}$$

The lower and upper bounds on the stresses in $P^{\gamma\in(0,1)}$ are not changed compared to P_N because of the damage condition. This choice can in practice be changed without any difficulties. The bounds on the eigenfrequencies are however allowed to change with the damage scenarios, just like in [44]. This option can be used to relax the design requirements for some damage scenarios. In practice this allows the system to operate under less severe requirements until the damage can be repaired or the damaged member(s) replaced.

For problems with damage scenarios where (parts of) members vanish the set of stress constraints is reduced such that no local stress constraints are included in points in the excluded (parts of) members. In this situation, we model the fail-safe problem as

$$\begin{aligned} \underset{\mathbf{v}\in\mathcal{F}}{\text{minimize}} \quad & m(\mathbf{v}) \\ \text{subject to} \quad & \underline{\boldsymbol{\sigma}} \leq \boldsymbol{\sigma}_e^{(j)}(\mathbf{v}) \leq \overline{\boldsymbol{\sigma}} \qquad \forall\, j \quad \forall\, e \in \mathcal{E} \setminus \mathcal{R}_j, \\ & \underline{f}_k^{(j)} \leq f_k^{(j)}(\mathbf{v}) \leq \overline{f}_k^{(j)} \quad \forall\, j \quad \forall\, k = 1, \ldots, p. \end{aligned} \tag{$P^{\gamma=1}$}$$

where $\mathcal{R}_j \subseteq \mathcal{D}_j \subseteq \mathcal{E}$ denotes the sub-set of completely damaged elements in the scenario j. Stress constraints are not imposed on the completely damaged elements since these elements are removed in the corresponding scenario.

The fail-safe problems $P^{\gamma\in(0,1)}$ and $P^{\gamma=1}$ contain the local stress constraints for all damage scenarios, and this is assumed to include the nominal design as well. Hence, if the bounds on the variables and constraints in problem P_N are identical to those in $P^{\gamma\in(0,1)}$ then the feasible set of $P^{\gamma\in(0,1)}$ is a sub-set of the feasible set of P_N.

The problems P_N, $P^{\gamma\in(0,1)}$, and $P^{\gamma=1}$ are generally non-convex optimization problems with continuous variables. They can all be infeasible if the requirements are too demanding. The situation that the nominal problem P_N has a non-empty feasible set and that either one or both of the fail-safe problems $P^{\gamma\in(0,1)}$ or $P^{\gamma=1}$ are infeasible is a possibility.

It is noted that the frequency constraints in the above formulations may lead to bad separation of the lowest eigen-frequency as discussed in [8], where a multi-objective optimization formulation is used to achieve a good separation of the lowest eigen-frequency.

3 Working-set algorithm and implementation

The working-set algorithm which is employed here combines the algorithms presented in [48] and [41]. The description is therefore kept brief. The working-set algorithm is based on solving a sequence of nonlinear optimization problems (sub-problems) of increasing size combined with an outer update scheme of the constraints to be considered in the next sub-problem. If a nonlinear constraint is added to the working-set, it stays in the working-set. This makes the working-set algorithm differ from the the classical active-set methods normally used for linearly constrained problems, see e.g. [21], where a constraint is generally removed from the active-set once it becomes inactive. While the working-set algorithm does not remove any chosen constraints, the number of chosen constraints is kept small by limiting the number of critical constraints added to the working-set in each outer iteration. In this study, two parameters ϵ and m are used to limit the number of selected critical constraints following the work of [48] and [41]. Consequently, in a sub-problem some critical constraints may not be included in the working-set. Later a large portion of these excluded critical constraints may become inactive and thus do not need to be further included in the working-set.

The initial problem only contains the linear constraints, i.e. all nonlinear constraints have been relaxed. The working-set for the nonlinear constraints is initialized to the empty set, $\mathcal{W}^0 = \emptyset$ and the outer iteration counter k is set to zero. The initial linear programming problem is not solved. Instead the starting point is used to provide a set of violated nonlinear constraints to include immediately and update the working-set. The first problem solved thus contains nonlinear constraints. Inner iterations correspond to applying a suitable solver for nonlinear optimization and attempting to find a point satisfying the first-order optimality conditions with the provided choice of included constraints, i.e. the working-set. For each sub-problem one of several possibilities can occur. If the solver suggests that a sub-problem is infeasible then the working-set algorithm terminates without success in finding a design that satisfies all the design requirements. Since the problems are non-convex in general, the infeasibility might be local, i.e. around the current approximation of the current iterate, rather than a property of the problem instance itself.

If a point satisfying optimality conditions is found for the current sub-problem, the following steps are taken. All nonlinear constraints are evaluated at the found point and thereafter normalized with the maximum value of the constraints if it is above one. A set of critical constraints are selected whose normalized values are larger than a prescribed threshold $-\epsilon$. The normalized nonlinear constraints are

$$\widetilde{g} = \frac{g - g_{max}}{\max\{g_{max}, 1\}} \tag{8}$$

where g denotes one arbitrary nonlinear constraint function, for example, one local stress constraint or eigen-frequency constraint, $\widetilde{g}$ denotes the normalized value of g, and g_{max} denotes the maximum value of all nonlinear constraints including the local stress constraints and the eigen-frequency constraints. In previous studies, the parameter ϵ is used in [48] and m is used in [41].

The constraints in the working-set are first excluded from the set of critical constraints. The remaining critical constraints are then sorted in decreasing order by their normalized values and their indices are stored in the set of critical constraints $\mathcal{V}^k$. The $\min\{m, |\mathcal{V}^k|\}$ most critical constraints, where m is a positive and user determined integer, are considered critical. In other words, two parameters ϵ and m are used to limit the number of selected critical constraints. Their values are chosen as $\epsilon = 0.5$ and $m = 30$ in the numerical results. The relatively large value of ϵ allows to add more constraints each iteration. The total number is thus mainly limited by m.

The set of selected critical constraints at outer iteration k is denoted $\mathcal{Q}^k$. The working-set is updated as $\mathcal{W}^{k+1} = \mathcal{W}^k \cup \mathcal{Q}^k$ and the outer iteration counter is incremented by one. The next sub-problem is solved. This is repeated until either the sub-problem is reported infeasible or no violated constraints are present. In the latter case the algorithm terminates with a feasible point to the original problem satisfying the first-order optimality conditions.

From the description of the working-set algorithm one can conclude that the number of included constraints in the working-set from one outer iteration to the other is non-decreasing. This implies that if, for a given outer iteration, the feasible set is non-empty and an optimal design is found, the objective value should be increased compared to the previous outer iteration. The sequence of objective function values is thus non-decreasing for global minimizers. If the objective function goes down from one outer iteration to the other there is a clear indication that the previous design was not a global optimum.

3.1 Implementation

The working-set algorithm, the finite element routines for the structural analysis, the design sensitivity analysis, the objective and constraint functions and their derivatives are implemented in Matlab version 2019a [47]. The continuous nonlinear optimization problems are solved by the interior-point algorithm implemented in the function `fmincon` which is part of the Matlab Optimization Toolbox version (Version 8.4) [47]. Default parameters and tolerances are used except the number of maximum iterations is 100, which is reached for only one sub-problem. If this limit is met the reported design is used for the next iteration in the working-set algorithm. The required iteration

Table 1: Material properties and geometry ranges of members.

	Property	Value	Unit
Material	Young's modulus (E)	210	GPa
	Yield stress ($\overline{\sigma}$ and $-\underline{\sigma}$)	355	MPa
	Mass density (ρ)	7850	kg/m^3
Geometry range	Outer diameter (d_i)	[1, 2]	m
	Thickness (t_i)	[0.01, 0.1]	m
	Ratio of outer diameter to thickness (d_i/t_i)	[16, 64]	–

number to solve one sub-problem is impacted by the scaling of the objective function. The numerical results are obtained by scaling the objective function with a factor of 1×10^{-3}.

Analytical gradients are provided for the nonlinear objective function and the nonlinear stress and eigenfrequency constraints. Each stress constraints is normalized with the corresponding stress limit. Each eigenfrequency constraints is normalized with the corresponding eigenfrequency limit when the value of the limit is larger than one.

The results are obtained on a laptop equipped with Intel Core i7-8650U processor running at 1.90 GHz and 16 GB memory without the use of any parallel computation.

4 Numerical experiments

The structures, loads and boundary conditions for the three examples are displayed in Fig. 2. Tubular members are represented by double lines to visualize both outer diameter and thickness of each member. Single nodal load is applied in Example I and III, whereas multiple nodal loads are used in Example II. The default loads for Example I, II and III are F_1 =100 $\times$ 10^6 N, F_2 =5 $\times$ 10^6 N, and F_3 =30 $\times$ 10^6 N, respectively. Higher load levels are occasionally used and given in the related results. The applied loads are intentionally chosen to be simple to enhance the possibilities to reproduce the results. They are also chosen to be sufficiently large to visualize the differences between the conventional designs and the corresponding fail-safe designs and are not necessarily representative for any application realistic loading scenario. The intention of Example I is to provide a simple benchmark model. Example II and III are intended to resemble the frame structures of high-rise building [5, 42, 43] and offshore jacket support structures [37, 32].

The material properties and geometry ranges are given in Table 1. The geometry ranges of outer diameter and thickness are prescribed as bounds on design variables, whereas the geometry range of the ratio of outer diameter to thickness is imposed as linear constraints.

A mesh convergence study of the stresses and the eigenfrequencies was performed. Each member is modelled using the classical two-node Euler-Bernoulli beam element, see e.g. [16],[17], [29]. The shape functions are Hermite interpolation functions which interpolate the coordinates and slopes of the two nodes of the beam element. Each

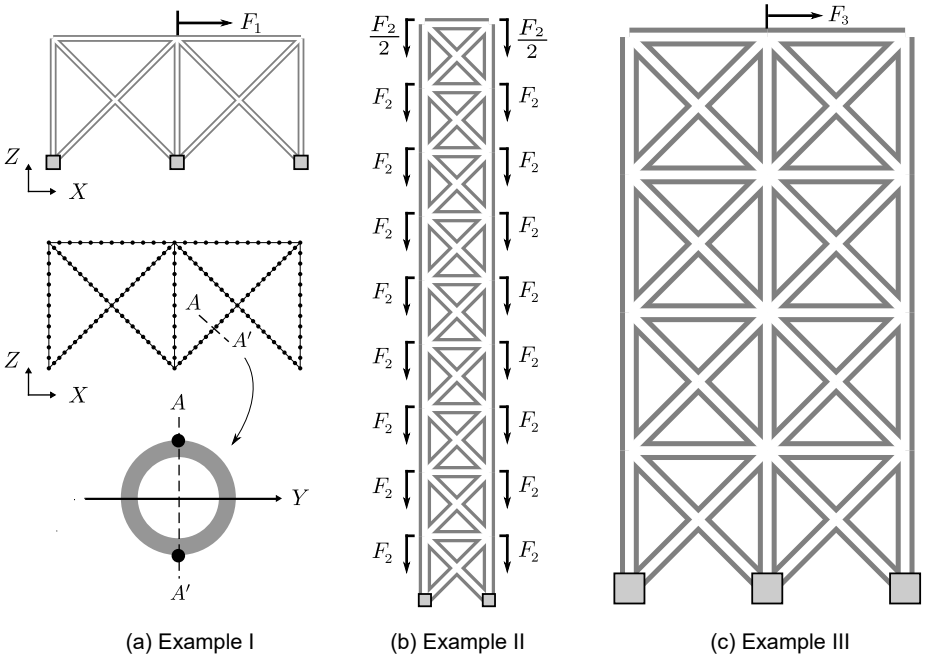

(a) Example I (b) Example II (c) Example III

Figure 2: Three tubular frame structures: the ground structures, loads, and boundary conditions. (a) Example I: $50\text{m} \times 25\text{m}$ domain with 13 members, the finite element model of beam elements, and the locations of the stresses (black dots) in the cross-section (gray hollow disk). (b) Example II: $25\text{m} \times 225\text{m}$ domain with 63 members (c) Example III: $50\text{m} \times 100\text{m}$ domain with 52 members. Grey squares denote the joints fixed to the ground.

member is uniformly discretized into 12 beam elements to ensure sufficiently accurate estimations of the stresses and eigen-frequencies. The length of the beam elements in the diagonal members is $\sqrt{2}$ times the length of the beam elements in the diagonal bracing members. The relative errors of the maximum stresses and the lowest eigenfrequencies are about 3% and 1×10^{-5}, respectively, with respect to the results obtained by using 80 elements per member. The convergence of the stress is also confirmed in comparison with the results from COMSOL Multiphysics, see Fig. 4. The stresses are evaluated at the two points of the cross-section at the midpoint of each element as illustrated by A and A' in Fig. 2(a).

For convenience of communication, the nominal optimization problem is denoted P_N. Three cases of the fail-safe optimization problem $P^{\gamma=1}$ are studied. These cover complete loss of up to one arbitrary member denoted $P_1^{\gamma=1}$, complete loss of up to two arbitrary members denoted $P_2^{\gamma=1}$, and complete loss of up to one arbitrary part of member denoted $P_{1,p}^{\gamma=1}$. Likewise, three cases of the fail-safe optimization problem $P^{\gamma\in(0,1)}$ are studied. Thickness degradation of one arbitrary member is denoted $P_1^{\gamma\in(0,1)}$, thickness degradation of up to two arbitrary members is denoted $P_2^{\gamma\in(0,1)}$, and thickness degradation of up to one arbitrary part is denoted $P_{1,p}^{\gamma\in(0,1)}$.

Table 2 shows the statistics of the finite element models of the structures and the optimization problems. The optimization problem $P_2^{\gamma=1}$ of Example III involves above 3 million local stress constraints and above 2 thousand eigenfrequency constraints.

The optimization problems $P_1^{\gamma=1}$ and $P_1^{\gamma\in(0,1)}$ include the nominal scenario and the damage scenarios with exactly one arbitrary member. The optimization problems $P_2^{\gamma=1}$ and $P_2^{\gamma\in(0,1)}$ includes the nominal scenario and the damage scenarios with exactly one arbitrary member and exactly two arbitrary members. The optimization problems $P_{1,p}^{\gamma=1}$ and $P_{1,p}^{\gamma\in(0,1)}$ include the nominal scenario and the damage scenarios with exactly one arbitrary part.

Let n denotes the number of members in a structure. The definition of members, parts and elements are illustrated in Fig. 1. A member is defined as an entire beam-like structure connecting two joints, and it can be discretized into a few elements for the purpose of analysis. The numbers of scenarios for $P_1^{\gamma=1}$ and $P_1^{\gamma\in(0,1)}$ are the same as $n+1$, including one nominal scenario and n damage scenarios where one member is completely or partially damaged in each damage scenario. The numbers of scenarios for $P_2^{\gamma=1}$ and $P_2^{\gamma\in(0,1)}$ are the same as $n(n-1)/2+n+1$, including one nominal scenario, n damage scenarios with one damaged member in each scenario, and $n(n-1)/2$ damage scenarios with two damaged members in each scenario. Given that each member consists of four parts, the numbers of scenarios for $P_{1,p}^{\gamma=1}$ and $P_{1,p}^{\gamma\in(0,1)}$ are the same as $4n+1$, including one nominal scenario and $4n$ damage scenarios.

Complete loss of (parts of) members reduces the number of required finite elements, the number of free degrees of freedom, and the number of stress constraints. Note that the internal nodes are removed when the damaged (parts of) members are removed. In contrast, thickness degradation of member or part does not reduce the number of finite elements, the number of free degrees of freedom, or the number of local stress constraints.

For the fail-safe optimization problem $P_1^{\gamma=1}$, the number of local stress constraints

is the product of the number of local stress constraints for one member, i.e. 96, and the square of the number of members, i.e. n^2. Similarly, one can replace n^2 with $(n^3 - n^2 + 2n)/2$ to compute the number of local stress constraints for the fail-safe optimization problem $P_2^{\gamma=1}$. For the fail-safe optimization problem $P_{1,p}^{\gamma=1}$, the number of local stress constraints is the product of the number of local stress constraints for one part, i.e. 24, and the square of the number of parts, i.e. $16n^2$. For the fail-safe optimization problems of $P_1^{\gamma\in(0,1)}$, $P_2^{\gamma\in(0,1)}$ and $P_{1,p}^{\gamma\in(0,1)}$, the number of local stress constraints is the product of the number of local stress constraints for the nominal scenario and the number of scenarios, since all scenarios have the same number of local stress constraints.

The number of eigenfrequency constraints is not given in Table 2. For each optimization problem, it is twice the number of damage scenarios. Each scenario involves a lower and upper bound on the lowest eigenfrequency, i.e. fundamental frequency.

The number of design variables is two times the number of members. All design variables are bounded from below and from above. The number of general linear constraints is also two times the number of members. These linear constraints model lower and upper limits on the diameter to thickness ratio in the members.

Table 3 shows the statistics of the set of numerical results. It shows that the working-set method generally requires a small number of sub-problems (e.g. ≤ 9) to solve the optimization problems. As a result, a small number of local stress constraints are included in the the working-sets. Note that the stress constraints are not aggregated and the included scenarios are the scenarios with at least one local stress constraint or eigen-frequency constraint in the scenario included in the working-set. For Example III with up to two arbitrary members removed, the final working-set includes local stress constraints amounting to 240 of the above 3.3 million local stress constraints, which is approximately 72 per million or 0.07‰. This demonstrates the proposed working-set algorithm is highly efficient to solve the fail-safe optimization problems. Each sub-problem is solved by calling the routines for computing the nonlinear constraints of stresses and eigenfrequencies a few times. The total number of these function calls of the nonlinear constraints are also displayed in the table.

The number of the activated local stress constraints in final design are determined by the normalized local stress constraints with a given tolerance of 1×10^{-6}. For the final designs, a few local stress constraints in the working-set are active.

4.1 Example I

Nominal design

For Example I, the optimal nominal design is shown in Fig. 3a. It has four large-thickness members forming essentially a two-beam structure where each beam has two members. The thickness values of the rest members are 0.015625 m, which corresponds to the smallest diameter of 1m and the largest ratio of diameter to thickness, i.e. 64.

The lowest eigenfrequencies of all the scenarios are bounded between [0, 20] Hz. These slack eigenfrequency constraints allow us to focus on the optimized design due

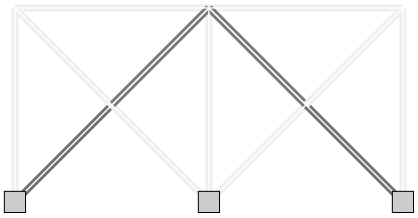

(a) Nominal design for P_N, $m = 1.72 \times 10^5$

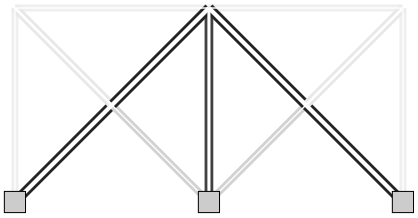

(b) Fail-safe design for $P_1^{\gamma=1}$, $m = 3.33 \times 10^5$

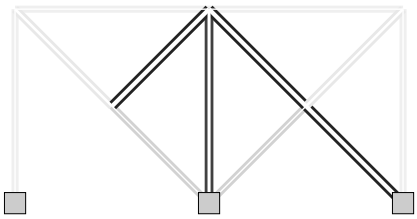

(c) Worst-case damage scenario for the design in (b).

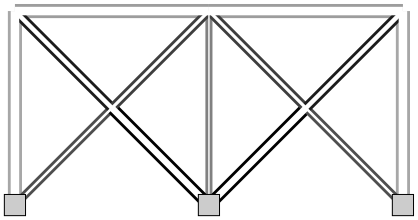

(d) Fail-safe design for $P_2^{\gamma=1}$, $m = 6.34 \times 10^5$

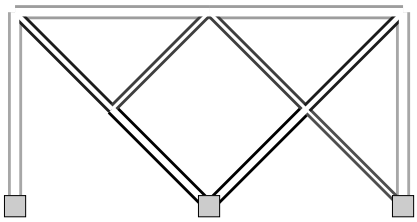

(e) Worst-case damage scenario for the design in (d).

Figure 3: The nominal and fail-safe optimized designs for Example I. (a) The nominal optimized design. (b) The fail-safe optimized design for removing up to one arbitrary member. (d) The fail-safe optimized design for removing up to two arbitrary members. (c) and (e) are the worst-case damage scenarios for the designs in (b) and (d). The width and grayness of the double line represent the diameter and thickness of the member, respectively.

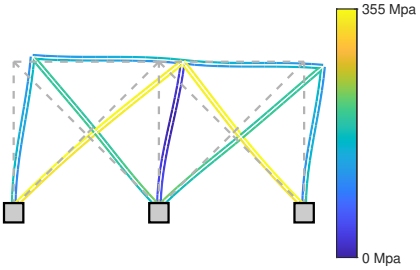

(a) Stress of nominal design in Fig. 2a

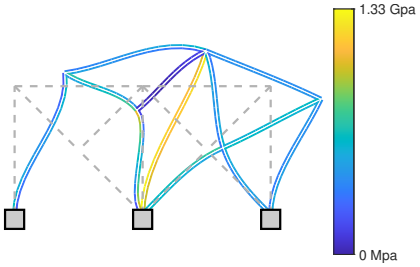

(b) Stress distribution for one damage scenario of nominal design in Fig. 2a

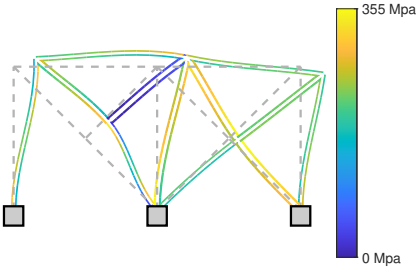

(c) Stress distribution for worst-case scenario of design in Fig. 3c

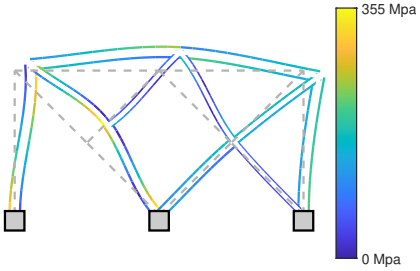

(d) Stress distribution for worst-case scenario of design in Fig. 3e

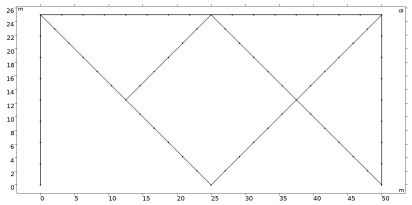

(e) Model of worst-case scenario of design in Fig. 3c built with COMSOL

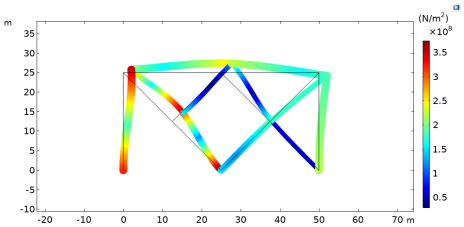

(f) Stress of worst-case scenario of design in Fig. 3c obtained with COMSOL

Figure 4: Stress distributions and displacements for the optimized designs for Example I. (a) The nominal design. (b) The displacements and stresses of the nominal design when one diagonal bar is removed. (c) the worst-case scenario of the fail-safe design for removing up to one arbitrary member. (d) The worst-case scenario of the fail-safe optimized design for removing up to two arbitrary members. (e) The stress magnitude of the worst-case scenario of the fail-safe design for removing up to two arbitrary members obtained by using COMSOL Multiphysics 5.5. In (a-c) the line color represents the stress magnitude $|\sigma|$ at two points in the mid-span cross-section of each beam element, for example, A and A' in Fig. 2a. In (e) the line color represents the maximum stress magnitude $|\sigma|$ in the cross-section of each beam element. The displacements in (a-d) are amplified by a factor of 50 for the purpose of visualization.

to the local stress constraints. The impact of the eigenfrequency constraints on the optimized design are studied later in this paper.

Complete loss of member(s)

The fail-safe design for $P_1^{\gamma=1}$ is shown in Fig. 3b. It consists of five thick members forming a three-beam structure where each diagonal beam has two members. The worst-case scenario is shown in Fig. 3c, where one bracing member is removed. Due to symmetry, there is another worst-case scenario.

The fail-safe design for $P_2^{\gamma=1}$ is shown in Fig. 3d. It is made of 9 large-thickness members and 4 large-diameter members. The worst-case scenario is shown in Fig. 3e, where one bracing member and one vertical member are removed. Similar to the case of $P_1^{\gamma=1}$, only one of the two equal worst-case scenarios is displayed due to symmetry.

The objective function values of the fail-safe designs for $P_1^{\gamma=1}$ and $P_2^{\gamma=1}$ are larger than that of the nominal design. In fail-safe designs, more large-thickness/diameter members are involved to present an increased complexity.

In order to provide an intuitive interpretation of the nominal design and the fail-safe optimized designs, the deformation and stress distribution of the designs in Fig. 3 are displayed in Fig. 4. It is seen that the members in the nominal design (Fig. 4a) and in the worst-case scenario of the fail-safe optimized design for $P_1^{\gamma=1}$ (Fig. 4c) mainly experience tension or compression, whereas the members in the worst-case scenario of the fail-safe optimized design for $P_2^{\gamma=1}$ (Fig. 4d) experience a combination of tension/compression and bending in the worst-case scenario. The stress distribution of the worst-case scenario of the design for $P_2^{\gamma=1}$ (Fig. 4d) is compared with the result obtained by using the commercial software COMSOL Multiphysics 5.5 (Fig. 4f). Note that the stress plot in COMSOL only provides one maximum stress for each cross-section, while our stress plots provide two stresses for each cross-section. Our result agrees well with the result from COMSOL in terms of the deformation, the maximum stress magnitude indicated by the scale of the colorbar and the spatial distribution of the section-wise maximum stress in the members.

Thickness degradation of member(s)

Two fail-safe optimized designs for $P_1^{\gamma\in(0,1)}$ are displayed in Fig. 5a and 5b. The thickness degradation levels are for these two examples set to $\gamma = 0.5$ and $\gamma = 0.9$, respectively. When the thickness degradation level is small and moderate (e.g. $\gamma = 0.5$), the fail-safe optimized designs are similar to the nominal design in Fig. 3a with an increased mass of material. When the degradation level is close to one (e.g. $\gamma = 0.9$), the fail-safe optimized design in Fig. 5b is similar to the fail-safe optimized design for $P_1^{\gamma=1}$ in Fig. 3b. However, the fail-safe optimized design for $\gamma = 0.9$ has a larger objective value than the fail-safe optimized design for $\gamma = 1$. This is due to the large stress in the damaged member as discussed in an analytical study [18].

The above observation also applies to the fail-safe optimized designs shown in Fig. 5c and 5d for $P_2^{\gamma\in(0,1)}$.

Loss and degradation of a part

Two fail-safe optimized designs for thickness degradation of one arbitrary part $P_{1,p}^{\gamma\in(0,1)}$ are displayed in Fig. 5e and 5f for the thickness degradation level $\gamma = 0.5$ and $\gamma = 0.9$, respectively. When the level of thickness degradation is small and moderate (e.g. $\gamma \leq 0.5$), the objective value of the fail-safe optimized design for $P_{1,p}^{\gamma\in(0,1)}$ is close to the corresponding objective values of the optimized designs for $P_1^{\gamma\in(0,1)}$ and $P_2^{\gamma\in(0,1)}$. When the level of thickness degradation is close to one (e.g. $\gamma = 0.9$), the objective value of the fail-safe optimized design for $P_{1,p}^{\gamma\in(0,1)}$ is larger than the objective function values for both $P_1^{\gamma\in(0,1)}$ and $P_2^{\gamma\in(0,1)}$. This indicates that a local thickness degradation in a member can cause a larger stress than the thickness degradation of an entire member.

From the point of view of the layout, a small and moderate degradation does not cause a change of the number of large-thickness/diameter members. When the degradation is severe, the number of large-diameter/thickness members increases. For a severe degradation, the optimized design for damage of one arbitrary part $P_{1,p}^{\gamma\in(0,1)}$ is more conservative than the design for damage of up to two arbitrary members $P_2^{\gamma\in(0,1)}$, which is more conservative than the design for damage of up to one arbitrary member $P_1^{\gamma\in(0,1)}$.

Note that the limit of the maximum diameter $d_{\max}$ is increased to $3\,\mathrm{m}$ in order to obtain the design for $P_{1,p}^{\gamma=0.9}$ in Fig. 5f, where all members reach the maximum limit of diameter except the middle vertical bar. For a fair comparison, the increased limit $d_{\max}$ is also applied in the optimization to obtain the designs for $P_1^{\gamma=0.9}$ and $P_2^{\gamma=0.9}$ in 5b and 5d.

The optimal fail-safe designs for complete loss of up to one arbitrary part $P_{1,p}^{\gamma=1}$ are the same as the designs for complete loss of up to one arbitrary member $P_1^{\gamma=1}$ when the prescribed eigen-frequency constraints are not active. This relation can be seen in Fig. 6 for $\gamma = 1$, where the objective values of $P_1^{\gamma=1}$ and $P_{1,p}^{\gamma=1}$ are the same.

Fig. 6 shows a comprehensive comparison of the objective function values of the optimized designs for different damage scenarios. When the thickness degradation level γ increases, the objective function values of the fail-safe optimized designs become larger than the objective value of the nominal design. As the thickness degradation level γ further increases, the objective function values of the fail-safe optimized designs for thickness degradation become even larger than the objective function values of the fail-safe optimized designs for complete loss of (parts of) members.

Impact of eigenfrequency constraint

Since one fail-safe optimization problem involves a number of scenarios, the lowest eigenfrequencies of the structure in all scenarios generally are not the same value similar to the case of stress. It may be challenging to require the lowest eigenfrequenies of all scenarios to be located in a small region in the frequency range.

A set of fail-safe optimized designs for thickness degradation of up to one arbitrary part $P_{1,p}^{\gamma=1}$ with varying lower bound on the eigenfrequency are displayed in Fig.

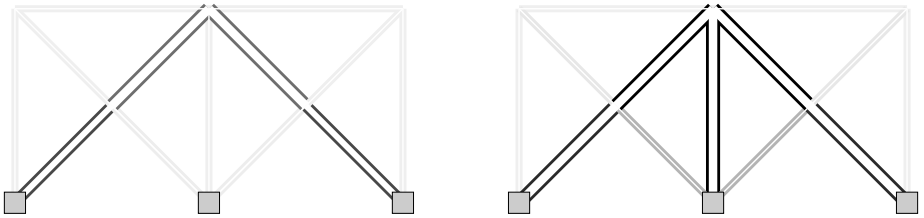

(a) $P_1^{\gamma=0.5}$, $m = 2.81 \times 10^5$

(b) $P_1^{\gamma=0.9}$, $m = 7.32 \times 10^5$

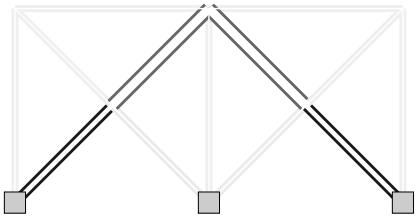

(c) $P_2^{\gamma=0.5}$, $m = 2.93 \times 10^5$

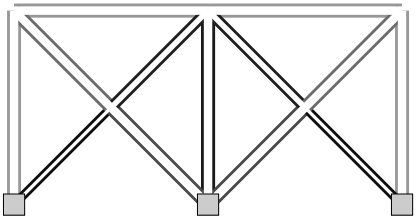

(d) $P_1^{\gamma=0.9}$, $m = 1.12 \times 10^6$

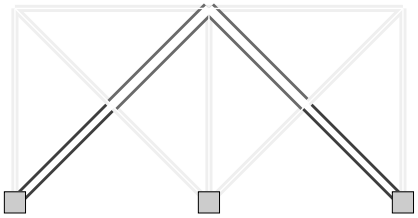

(e) $P_{1,p}^{\gamma=0.5}$, $m = 2.89 \times 10^5$

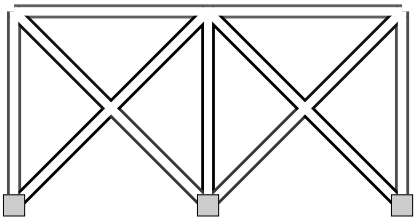

(f) $P_{1,p}^{\gamma=0.9}$, $m = 1.62 \times 10^6$

Figure 5: Fail-safe optimized designs for Example I with damage scenarios of thickness degradation of member or part. (a-b) thicknesses degradation of up to one arbitrary member $P_1^{\gamma\in(0,1)}$. (c-d) thickness degradation of up to two arbitrary members $P_2^{\gamma\in(0,1)}$. (e-f) thickness degradation of one arbitrary part $P_{1,p}^{\gamma\in(0,1)}$. The width and grayness of the double line represent the diameter and thickness of the member, respectively.

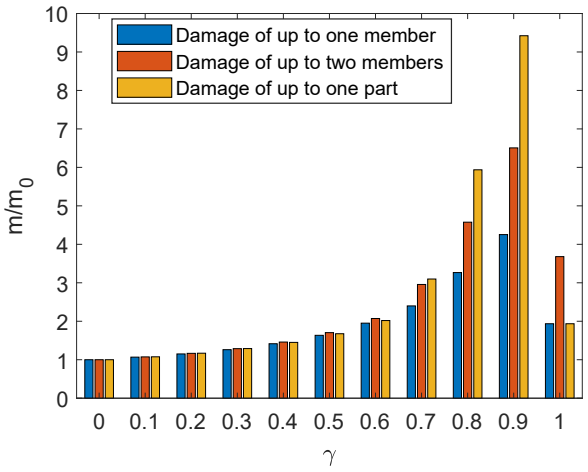

Figure 6: Comparison of the objective values of the nominal and fail-safe optimized designs of Example I with different damage scenarios and different levels of degradation γ. The objective function values m are normalized with the objective value of the nominal design m_0.

7. As the lower bound of eigenfrequency increases, the objective value of the optimized design increases, and the number of large-diameter members also increases. The increasing number of large-diameter members indicates that the optimized design is more and more influenced by the bending motion because a large-diameter member has a larger bending stiffness compared to a small-diameter member when their areas of the cross-section are the same.

When the lower bound of eigenfrequency is smaller than 5 Hz the optimized design is driven by both local stress constraints and eigenfrequency constraints. When the lower bound of eigenfrequency is 5 Hz, the optimized design in Fig. 7f is dominated by the eigenfrequency constraints, while all local stress constraints are not active.

The impact of eigenfrequency constraints on the optimized design is due to the critical vibration mode shown in Figs. 7g and 7h, where a local vibration occurs in the free end and the linked joint and members.

Note that the vibration problem caused by the free end also occurs in the damage scenarios for complete loss of up to two arbitrary members $P_2^{\gamma=1}$. Fig. 8a shows an fail-safe optimized design for $P_2^{\gamma=1}$ with an increased lower bound of eigenfrequency, 3Hz. The optimized design has a large objective value than the design shown in 3d. The critical vibration mode is shown in Fig. 8b.

4.2 Example II

This example resembles a tubular frame in the high-rise building [42, 43, 52, 5]. High-rise building is one of the applications with high concern of structural safety. This example is used to further compare the conventional optimized design and the fail-safe

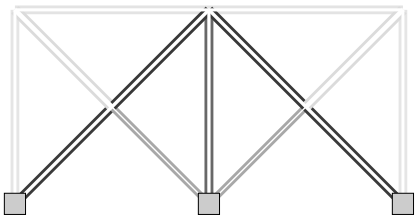

(a) $P_{1,p}^{\gamma=1}$, [3, 9.66] Hz, $m = 3.35 \times 10^5$

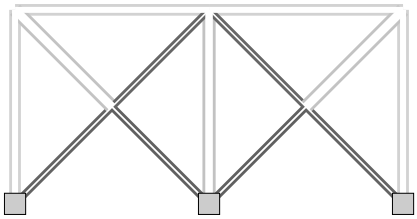

(b) $P_{1,p}^{\gamma=1}$, [4, 11.49] Hz, $m = 3.58 \times 10^5$

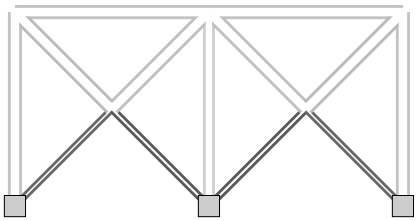

(c) $P_{1,p}^{\gamma=1}$, [4.5, 13.41] Hz, $m = 4.06 \times 10^5$

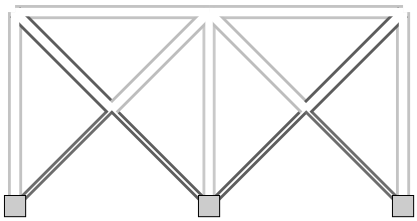

(d) $P_{1,p}^{\gamma=1}$, [4.8, 13.36] Hz, $m = 4.62 \times 10^5$

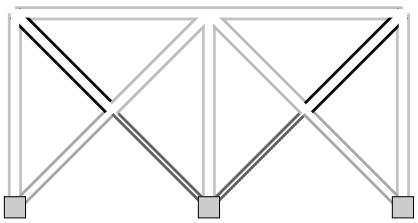

(e) $P_{1,p}^{\gamma=1}$, [4.96, 12.94] Hz, $m = 5.20 \times 10^5$

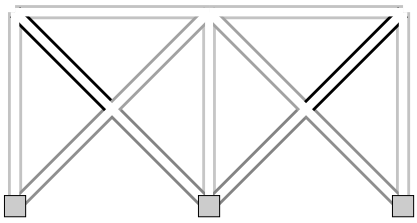

(f) $P_{1,p}^{\gamma=1}$, [5, 13.95] Hz, $m = 6.01 \times 10^5$

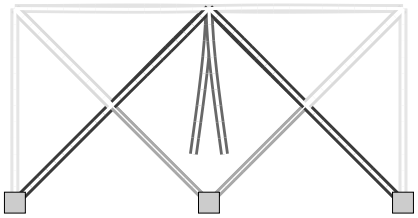

(g) The most critical vibration mode of (a), 3 Hz.

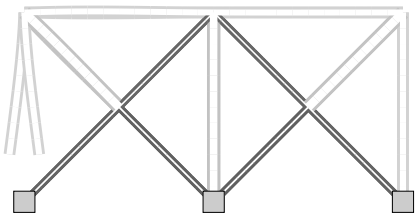

(h) The most critical vibration mode of (b), 4 Hz.

Figure 7: Impact of the frequency limits on the fail-safe optimized designs for Example I with damage scenarios of complete damage of up to one arbitrary part $P_{1,p}^{\gamma=1}$. (a-f) Optimized design with different lower bounds of eigenfrequency. The upper bound on the eigenfrequency is 20 Hz. $F_1 = 1 \times 10^8$ N. The eigenfrequency range under the sub-figure shows the real eigenfrequency range of all scenarios of the optimized design. (g-h) The most critical vibration modes of the optimized designs in (a-b). Two states are shown in an overlapped way for each vibration mode to illustrate the vibration motion.

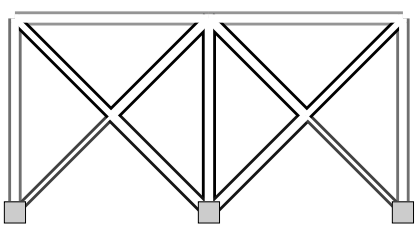

(a) Fail-safe optimized design for $P_2^{\gamma=1}$, [3, 13.29] Hz, $m = 8.99 \times 10^5$

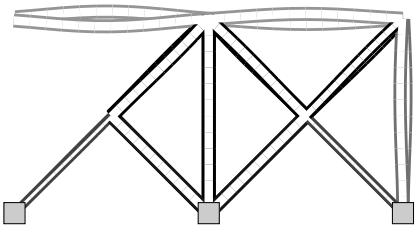

(b) Vibration mode of the worst-case scenario of (a), 3 Hz.

Figure 8: One optimized design for Example I with damage scenarios of complete loss of up to two arbitrary members $P_2^{\gamma=1}$ and the eigenfrequency limit of [3, 20] Hz.

optimized design.

Nominal design

For the nominal designs, as the load level increases, the vertical members (i.e. the legs) become larger in thickness than the bracing members.

Fail-safe design

For the fail-safe optimized designs, the bracing members become thicker than the vertical members. As the load further increases, the bracing members become larger in diameter than the vertical members. In comparison to the nominal design, the fail-safe design features large-thickness/diameter bracing members.

Fig. 10 shows a comparison of the displacements and stresses of the nominal design in Fig. 9b and the fail-safe design in Fig. 9c when one bar is removed. The applied load is $F_2 = 5 \times 10^6$ N. It is seen that when one bar (i.e. one of the legs on the ground) is removed, the nominal design has larger displacements than the fail-safe design. The maximum stress in the nominal design is about 5 times of the maximum stress in the fail-safe design.

For this example, it is challenging to obtain the fail-safe design for $P_2^{\gamma=1}$, because of its simple layout. When removing one leg and one bracing member at one joint on the ground, the structure stands on the ground through the other joint, making it difficult to resist the bending loads.

4.3 Example III

Nominal designs

Three nominal designs for three levels of applied loads are displayed in Fig. 11a, 11b, and 11c. As the load level increases, the vertical members become thicker in thickness. As the load level further increases, the bracing members at the top and bottom become larger in thickness or diameter. The number of large-thickness/diameter members grows, as the magnitude of the load increases.

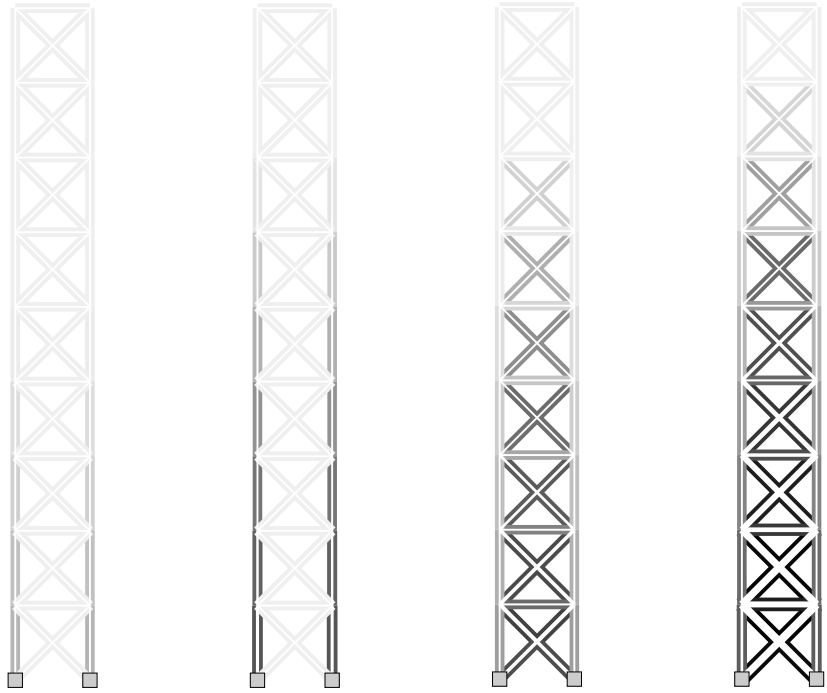

(a) P_N, $F_2 = 5 \times 10^6$, $m = 5.63 \times 10^5$.

(b) P_N, $F_2 = 1 \times 10^7$, $m = 7.65 \times 10^5$.

(c) $P_1^{\gamma=1}$, $F_2 = 5 \times 10^6$, $m = 1.19 \times 10^6$.

(d) $P_1^{\gamma=1}$, $F_2 = 8 \times 10^6$, $m = 1.97 \times 10^6$.

Figure 9: The nominal and fail-safe optimized designs for Example II. (a-b) The nominal optimized designs P_N with two load levels. (c-d) The fail-safe optimized designs with damage scenarios of removing up to one arbitrary member $P_1^{\gamma=1}$ at two load levels.

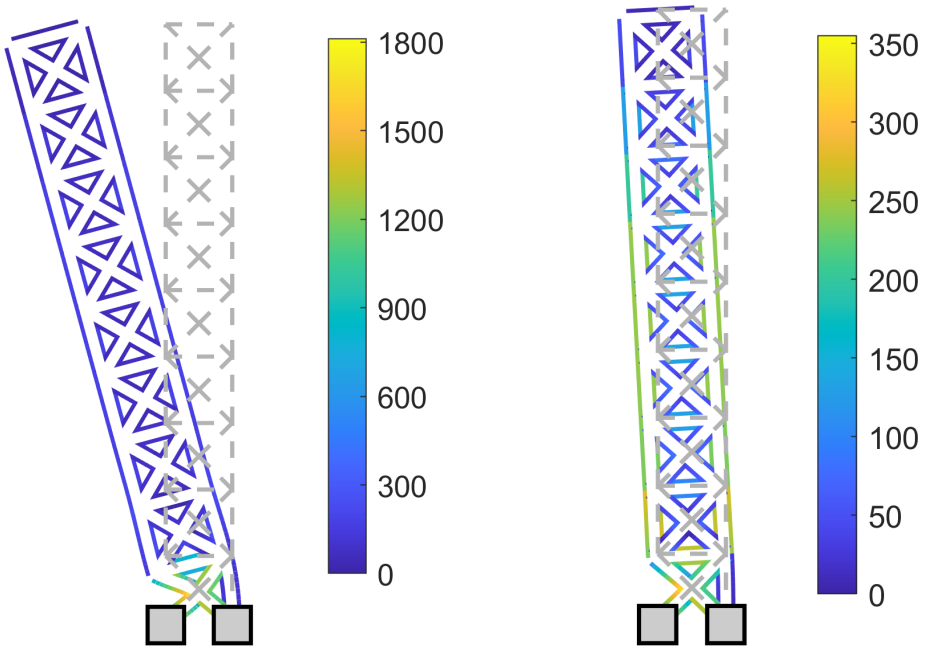

(a) Nominal design in Fig. 9b

(b) Fail-safe design in Fig. 9c.

Figure 10: Comparison of the displacements and stresses of the nominal design in Fig. 9b and the fail-safe design in Fig. 9c when one bar is removed. The applied load is $F_2 = 5 \times 10^6$ N. The dashed lines display the initial configuration. The solid double lines denote the deformed configuration. The displacements are amplified with a factor of 10. The color of the double lines denotes the magnitude of the stresses. The colorbar for the stress is in MPa.

Complete loss of member(s)

The fail-safe designs for complete loss of one arbitrary member $P_1^{\gamma=1}$ are displayed in Fig. 11d and 11e. One worst-case scenario is shown in Fig. 11f for the fail-safe optimized in Fig. 11e. The fail-safe design for the load level $F_3 = 1 \times 10^7$ N is not obtained in the study because it exceeded the prescribed maximum iteration limit of 100 when solving a sequence of sub-problems.

One fail-safe design for complete loss of up to two arbitrary members $P_2^{\gamma=1}$, is displayed in Fig. 13a. Two worst-case scenarios are shown in Fig. 13b and 13c. The fail-safe design for $P_2^{\gamma=1}$ is similar to the fail-safe design of $P_1^{\gamma=1}$ except two large-diameter vertical members at the mid-span.

In contrast to the nominal designs, the fail-safe designs for $P_1^{\gamma=1}$ and $P_2^{\gamma=1}$ feature different geometric patterns featuring an increased number of large-thickness bracing members and large-thickness/diameter vertical members in the middle column.

This example implies that the nominal designs with an increased load level, which is equivalent to a larger safety factor, cannot replace the fail-safe optimized designs. For example, we compare the nominal design in Fig. 11c and the fail-safe design in Fig. 11d. The comparison is shown in Fig. 12. The nominal design in Fig. 11c has about 1.4 times mass compared to the fail-safe design in Fig. 11d. In this case, the nominal design and the fail-safe design have similar displacements. However, the nominal design in Fig. 11d shows a maximum stress of 900 MPa when one of the vertical thick bars at the bottom is removed, while the stresses in the fail-safe design in Fig. 11d fall within the stress limit of 355 MPa for all damage scenarios of removing up to one arbitrary member $P_1^{\gamma=1}$ due to the formulation of the fail-safe optimization problem.

Fig. 14 further compares the nominal design in Fig. 11c and the fail-safe design in Fig. 13a when two members are removed. Though the nominal design is obtained with a larger load, both its displacements and stresses are larger than those of the fail-safe design. Fig. 14c and 14d illustrate that the fail-safe design can effectively resist the applied load when two members are removed.

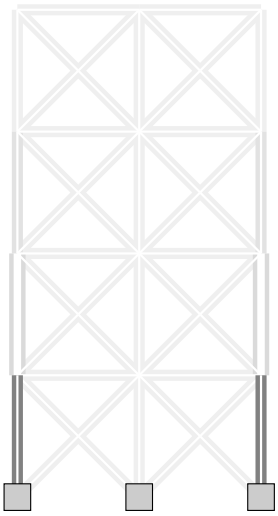

(a) Nominal design, $F_3 = 3\times 10^7$, $m = 4.77\times 10^5$.

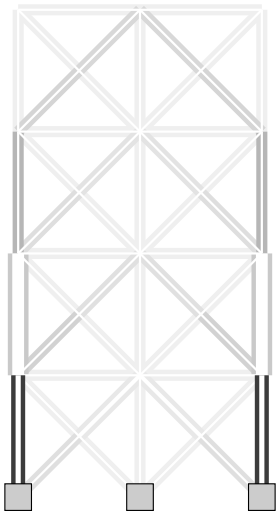

(b) Nominal design, $F_3 = 5\times 10^7$, $m = 6.17\times 10^5$.

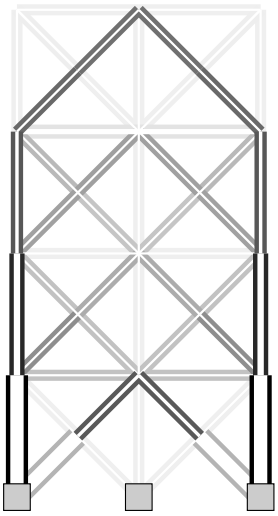

(c) Nominal design, $F_3 = 1\times 10^8$, $m = 1.16\times 10^6$.

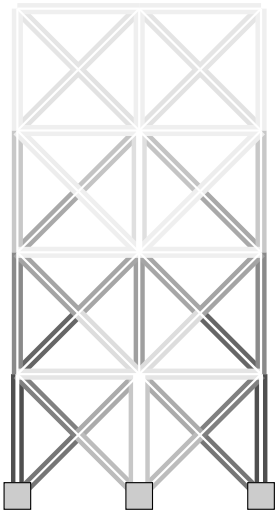

(d) Fail-safe design for $P_1^{\gamma=1}$, $F_3 = 3\times 10^7$, $m = 8.29\times 10^5$.

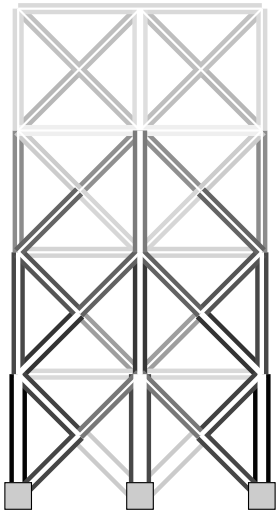

(e) Fail-safe design for $P_1^{\gamma=1}$, $F_3 = 5\times 10^7$, $m = 1.42\times 10^6$.

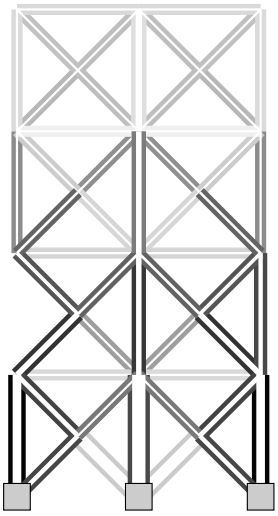

(f) The worst-case damage scenario of (e).

Figure 11: The nominal and fail-safe optimized designs for Example III. (a-c) The nominal designs for three load levels. (d-e) The fail-safe optimized designs with damage scenarios of removing up to one arbitrary member $P_1^{\gamma=1}$ for two load levels. (f) The worst-case damage scenario for the design in (e).

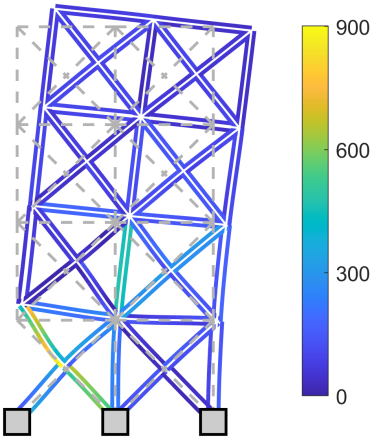

(a) Nominal design in Fig 11c.

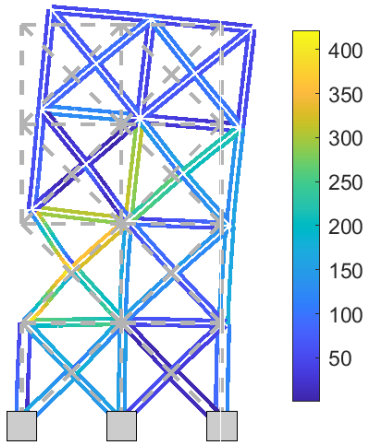

(b) Nominal design in Fig 11c.

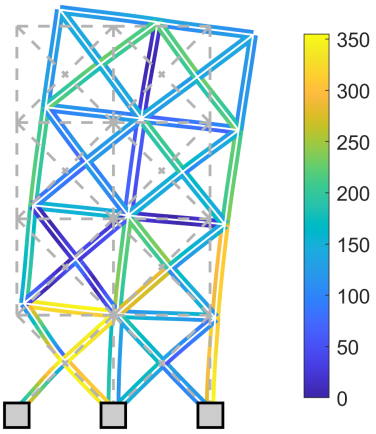

(c) Fail-safe design in Fig 11d.

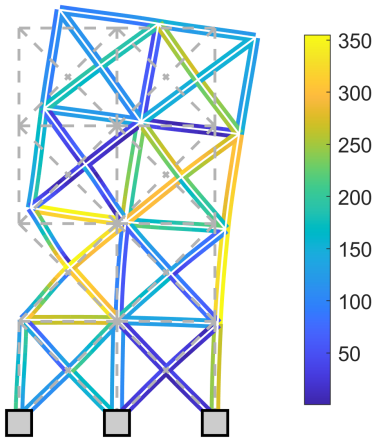

(d) Fail-safe design in Fig 11d.

Figure 12: Comparison of the displacements and stresses of the nominal design in Fig. 11c and the fail-safe design in Fig. 11d when one bar is removed. The applied load is $F_3 = 3 \times 10^7$ N. The dashed lines display the initial configuration. The solid double lines denote the deformed configuration. The displacements are amplified with a factor of 20. The color of the double lines denotes the magnitude of the stresses. The unit of the colorbar for the stress is in MPa.

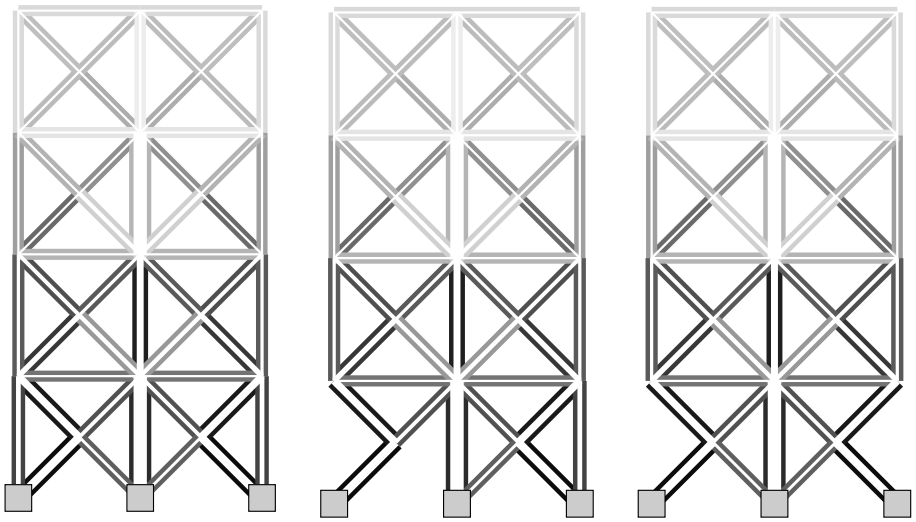

(a) Fail-safe design for $P_2^{\gamma=1}$, $F_3 = 3 \times 10^7$, $m = 1.55 \times 10^6$.

(b) First worst damage scenario of the design in (a).

(c) Second worst damage scenario of the design in (a).

Figure 13: (a) The fail-safe design for Example III with damage scenarios of removing up to two arbitrary members $P_2^{\gamma=1}$. (b-c) The first and second worst-case damage scenarios of the design in (a).

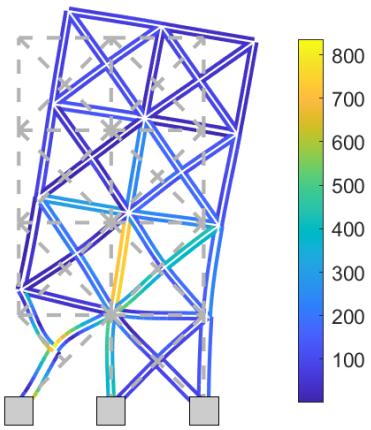

(a) Nominal design in Fig 11c.

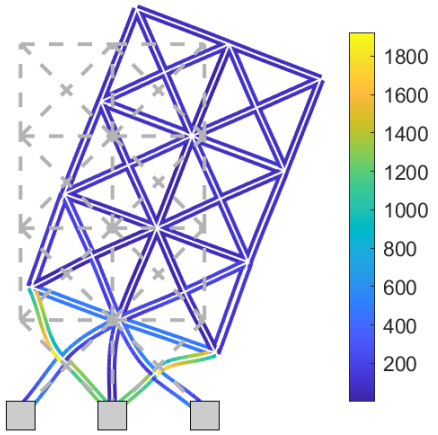

(b) Nominal design in Fig 11c.

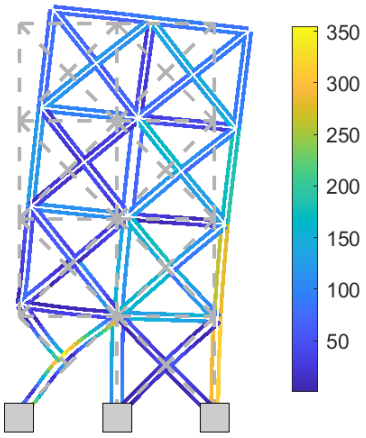

(c) Fail-safe design in Fig 13a.

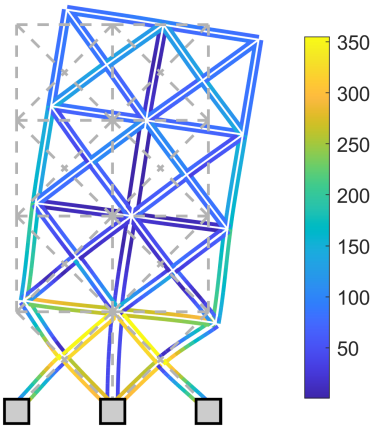

(d) Fail-safe design in Fig 13a.

Figure 14: Comparison of the displacements and stresses of the nominal design in Fig. 11c and the fail-safe design in Fig. 13a when one bar is removed. The applied load is $F_3 = 3 \times 10^7$ N. The dashed lines display the initial configuration. The solid double lines denote the deformed configuration. The displacements are amplified with a factor of 20. The color of the double lines denotes the magnitude of the stresses. The unit of the colorbar for the stress is in MPa.

Table 2: Statistics of the structures and the optimization problems. P_N: nominal design. $P_1^{\gamma=1}$: complete loss of up to one arbitrary member. $P_2^{\gamma=1}$: complete damage of up to two arbitrary members. $P_{1,p}^{\gamma=1}$: complete loss of up to one arbitrary part of member. $P_1^{\gamma\in(0,1)}$: thickness degradation of up to one arbitrary member. $P_2^{\gamma\in(0,1)}$: thickness degradation of up to two arbitrary members. $P_{1,p}^{\gamma\in(0,1)}$: thickness degradation of up to one arbitrary part of member.

	Problem	Members	Elements	Free DOFs	Scenarios	Stress constraints
I	P_N	13	156	444	1	624
	$P_1^{\gamma=1}$	12/13	144/156	411/444	14	8112
	$P_2^{\gamma=1}$	11/12/13	132/144/156	378/411/444	92	49296
	$P_{1,p}^{\gamma=1}$	13	153/156	438/444	53	32448
	$P_1^{\gamma=0.5}$	13	156	444	14	8736
	$P_2^{\gamma=0.5}$	13	156	444	92	57408
	$P_{1,p}^{\gamma=0.5}$	13	156	444	53	33072
II	P_N	63	756	2160	1	3024
	$P_1^{\gamma=1}$	62/63	744/756	2127/2160	64	190512
III	P_N	52	624	1776	1	2496
	$P_1^{\gamma=1}$	51/52	612/624	1743/1776	53	129792
	$P_2^{\gamma=1}$	50/51/52	600/612/624	1710/1743/1776	1379	3312192

Table 3: Statistics of a set of numerical results of the fail-safe designs with the working-set method for Example I, II and III. P_N: nominal design. $P_1^{\gamma=1}$: complete loss of up to one arbitrary member. $P_2^{\gamma=2}$: complete loss of up to two arbitrary members. $P_{1,p}^{\gamma=1}$: complete loss of up to one arbitrary part of member. $P_2^{\gamma\in(0,1)}$: thickness degradation of up to one arbitrary member. $P_2^{\gamma\in(0,1)}$: thickness degradation of up to two arbitrary members. $P_{1,p}^{\gamma\in(0,1)}$: thickness degradation of up to one arbitrary part of member. The loads, objective values and CPU time are in 1×10^6 N, 1×10^6 kg, and second, respectively.

				Stress constraints		Eig. cons.	Scenarios		Results		
	Problem	F	Frequency	incl.	act.	(incl., act.)	(incl., act.)	Prob.	Calls	CPU	obj.
I	P_N	100	[0,20]	30 (4.8%)	26	(0, 0)	(1, 1)	2	17	0.7	0.17
	$P_1^{\gamma=1}$	100	[0,20]	90 (1.1%)	8	(0, 0)	(12, 2)	4	99	6.9	0.33
	$P_2^{\gamma=1}$	100	[0,20]	120 (0.2%)	14	(0, 0)	(47, 8)	5	126	20.3	0.63
	$P_{1,p}^{\gamma=1}$	100	[0,20]	90 (0.3%)	32	(0, 0)	(24, 8)	4	88	12.4	0.33
	$P_1^{\gamma=0.5}$	100	[0,20]	60 (0.7%)	4	(0, 0)	(4, 4)	3	56	1.9	0.28
	$P_2^{\gamma=0.5}$	100	[0,20]	90 (0.2%)	6	(0, 0)	(22, 5)	4	54	8.8	0.29
	$P_{1,p}^{\gamma=0.5}$	100	[0,20]	60 (0.2%)	6	(0, 0)	(16, 6)	3	26	3.2	0.29
	$P_1^{\gamma=0.9}$	100	[0,20]	30 (0.3%)	4	(0, 0)	(4, 4)	2	35	1.7	0.73
	$P_2^{\gamma=0.9}$	100	[0,20]	90 (0.2%)	12	(0, 0)	(13, 8)	4	84	7.1	1.12
	$P_{1,p}^{\gamma=0.9}$	100	[0,20]	60 (0.2%)	8	(0, 0)	(8, 3)	3	72	7.7	1.62
	$P_{1,p}^{\gamma=1}$	100	[3,20]	144 (0.4%)	16	(6, 0)	(30, 8)	6	161	59.4	0.33
	$P_{1,p}^{\gamma=1}$	100	[4,20]	80 (0.2%)	32	(10, 5)	(48, 37)	4	64	33.8	0.36
	$P_{1,p}^{\gamma=1}$	100	[4.5,20]	50 (0.2%)	24	(10, 3)	(34, 27)	3	58	25.5	0.41
	$P_{1,p}^{\gamma=1}$	100	[4.8,20]	76 (0.2%)	24	(12, 3)	(44, 27)	4	51	26.0	0.46
	$P_{1,p}^{\gamma=1}$	100	[4.96,20]	68 (0.2%)	24	(12, 5)	(44, 29)	4	124	59.2	0.52
	$P_{1,p}^{\gamma=1}$	100	[5,20]	38 (0.1%)	0	(12, 5)	(38, 5)	3	547	216.9	0.60
	$P_2^{\gamma=1}$	100	[3,20]	86 (0.3%)	4	(4, 4)	(34, 8)	4	154	29.6	0.90
II	P_N	5	[0,20]	149 (4.9%)	10	(1, 0)	(1, 1)	6	134	14.4	0.56
	P_N	10	[0,20]	240 (7.9%)	14	(0, 0)	(1, 1)	9	443	56.7	0.76
	$P_1^{\gamma=1}$	5	[0,20]	240 (0.1%)	40	(0, 0)	(39, 26)	9	247	234.3	1.19
	$P_1^{\gamma=1}$	8	[0,20]	300 (0.2%)	48	(0, 0)	(48, 29)	11	366	398.3	1.97
III	P_N	30	[0,20]	90 (3.6%)	6	(0, 0)	(1, 1)	4	71	5.6	0.48
	P_N	50	[0,20]	210 (8.4%)	22	(0, 0)	(1, 1)	8	229	23.9	0.62
	P_N	100	[0,20]	240 (9.6%)	22	(0, 0)	(1, 1)	9	822	119.6	1.16
	$P_1^{\gamma=1}$	30	[0,20]	210 (0.2%)	38	(0, 0)	(18, 14)	8	300	119.6	0.83
	$P_1^{\gamma=1}$	50	[0,20]	240 (0.2%)	46	(0, 0)	(20, 16)	9	1169	566.8	1.42
	$P_2^{\gamma=1}$	30	[0,20]	240 (0.007%)	44	(0, 0)	(46, 25)	9	631	707.8	1.55

5 Discussion

The damage scenario concerning partial degradation of member is re-visited, and the risk of obtaining an overly conservative design is pointed out. Another new damage scenario concerning complete or partial damage of parts of members is studied. Partial damage of one part of an arbitrary member can cause a higher cost design to satisfy the local stress constraints even than completely removing two arbitrary members. Complete loss of one part of an arbitrary member can cause lower frequency localized vibration modes than partial degradation or complete removal of one arbitrary member. Additionally, this kind of partial length loss damage is unique to fail-safe frame structure. In topology optimization of continuum structures, there is no a clear definition of member. Both member and its part can be described by a patch consisting of a few elements. Currently, very little research has considered low frequency local vibration modes in fail-safe topology optimization. The resulting structures may thus not be reliable when they are operated in a dynamic environment. Du et al. studied fail-safe topology optimization with fundamental frequency constraints in [19]. They experience similar lower frequency localized vibration modes due to free ends as reported in Table 1 and Figure 9b of [19].

The working-set algorithm is intended for problems with a relatively small number of design variables, but a large number of nonlinear constraints. For problems with this characteristics, it can be argued that the number of active nonlinear constraints at an optimum is likely to be small. The working-set algorithm can be combined with essentially any implementation of optimization method capable of providing points satisfying the first-order optimality conditions for the reduced problem and is as such easy to implement. The main motivation described here for the use of this kind of working-set algorithm is thus similar to the arguments presented in [48] and [41]. The considered problems generally do not have a large portion of the constraints active at the final design, i.e. most of the constraints are not design driving (although this cannot be guaranteed). The proposed working-set approach thus gives the possibility to reduce the memory requirements and computational cost in the optimization method and to also reduce the computational cost in the design sensitivity analysis. Table 4 displays a comparison of the computational time using the working-set method and using all the stress constraints for Example I. A speedup factor of 80 is achieved for $P_2^{\gamma=1}$. A larger speedup factor is expected when eigen-frequency constraints are involved and when the number of constraints further increases as in Examples II and III. For structural optimization problems not satisfying the stated requirements on the number of design variables and constraints, this approach is likely inadequate.

Table 4: Comparison of computational time in seconds using the working-set method and including all the stress constraints for the designs displayed in Fig. 3.

Problem	P_N	$P_1^{\gamma=1}$	$P_2^{\gamma=1}$
All stress constraints	1.3	23.2	1639.6
Working-set algorithm	0.7	6.9	20.3
Speedup factor	1.9	3.4	80.8

Compared to the fail-safe design problems considered in e.g. [44], the problems proposed here are simplified in terms of the versatility of the constraints. Our fail-safe problems do not include compliance requirements, nodal displacement constraints, member buckling constraints and other important constraints. It is however not expected that these types of constraints will create additional difficulties in practice. Displacement constraints are important as service limit states in practical engineering applications. Design sensitivities of displacement constraints are readily available, see e.g. [33]. The buckling constraints create theoretical and computational difficulties in truss topology optimization through "chains in compression" [1, 2, 3]. This complicating situation does not apply for the considered problems since they are sizing problems and the topology of the structure is known also for all damage scenarios. Even so, buckling constraints may become active at the optimal design.

The example problems that are modelled and solved are not particularly large in terms of the number of design variables or degrees of freedom. The number of constraints is however much larger than the number of variables. The problems can still in practice be modelled and solved with all constraints included using off-the-shelf optimization software intended for general purpose nonlinear programming as illustrated in Table 4. The number of local stress constraints in the examples could be increased substantially by expanding the number stress evaluation points. One could also consider transient loads with local stress constraints at each time-integration point as is done in [48]. Both of these actions result in problem instances of sufficient size to challenge general purpose methods both in terms of memory requirements and computational expenses. Based on the numerical results presented in [48] using a similar working-set approach applied to problems with millions of local stress constraints, it is reasonable to assume that the working-set approach may work in a similar fashion for fail-safe problems and that only a small fraction of the local stress constraints are included in the final working-set.

6 Conclusion

The numerical results demonstrate that local stress constraints should be modelled with care in fail-safe structural optimization. Similar issues as for stress-constrained topology optimization, i.e. the stress singularity issue, may occur. The objective function may rise significantly as the amount of degradation approaches complete removal of one or more members. This was studied for a small-scale academic example in [18]. Here, we numerically illustrate that it can occur for more realistic design situations. It is therefore important to remove local stress constraints in the relevant positions in the structure for damage scenarios involving removal of members or parts of members.

This study also provides an estimation of the mass of the fail-safe optimized design in comparison to the mass of the nominal design. Stress-constrained fail-safe design considering complete loss of up to one arbitrary member requires, in the studied examples, about 1.7 to 2.3 times the mass of the nominal design. The stress-constrained fail-safe design examples considering complete loss of up to two arbitrary members requires about 3.2 to 3.7 times the mass of the nominal design.

The numerical results indicate that completely removing one arbitrary part or two

arbitrary members can cause low frequency localized vibration modes. A stiffer structure is thus required to increase the lowest eigenfrequency among all the damage scenarios to satisfy the imposed frequency constraints.

The working-set algorithm requires a relatively modest number of sub-problems to be solved for the considered problem instances. Additionally, only a relatively small fraction of the local stress constraints and damage scenarios are included in the final working-set. A large number of local stress constraints are thus not close to active at the obtained designs. The working-set algorithm increases the computational efficiency to solve the fail-safe optimization problem, and reduces the requirement of large memory when dealing with millions of constraints compared to the situation that all constraints are included.

The numerical results illustrate that the nominal design with an increased load level, i.e. a larger safety factor, cannot replace the fail-safe design approach in certain situations. Without inclusion of the damage scenarios, the nominal design with an increased mass can still violate the local stress constraints when damage occurs.

Acknowledgements

The authors would like to thank our colleague Nicolò Pollini at DTU Wind Energy for generously providing constructive comments and suggestions for improvements on a draft manuscript.

The authors extend their sincere thanks to the three reviewers for providing relevant and constructive comments and suggestions on the manuscript.

Conflicts of interests

The corresponding author states that there are no conflicts of interest.

Replication of results

The numerical experiments are defined completely through the provided descriptions of the considered structural analysis and degradation models, the statements of the optimal design problems, the topology and geometry of the ground structures, the definition of the external loads, the material properties, and the limits on variables and constraints. The numerical results are obtained after solving a sequence of non-convex optimization problems. It is thus reasonable to expect that a different choice of optimization solver, solver parameters and tolerances, starting points, and working-set parameters can result in different final designs and iteration histories than presented herein.

References

[1] W. Achtziger. Local stability of trusses in the context of topology optimization Part I: Exact modelling. *Structural Optimization*, 17(4):235–246, 1999.

[2] W. Achtziger. Local stability of trusses in the context of topology optimization Part II: A numerical approach. *Structural Optimization*, 17(4):247–258, 1999.

[3] W. Achtziger. Optimization with variable sets of constraints and an application to truss design. *Computational Optimization and Applications*, 15(1):69–96, 2000.

[4] W. Achtziger and M.P. Bendsøe. Design for maximal flexibility as a simple computational model of damage. *Structural Optimization*, 10(3-4):258–268, 1995.

[5] M. Aldwaik and H. Adeli. Advances in optimization of highrise building structures. *Structural and Multidisciplinary Optimization*, 50(6):899–919, 2014.

[6] O. Ambrozkiewicz and B. Kriegesmann. Density-based shape optimization for fail-safe design. *Journal of Computational Design and Engineering*, 7(5):615–629, 2020.

[7] J.S. Arora, D.F. Haskell, and A.K. Govil. Optimal design of large structures for damage tolerance. *AIAA Journal*, 18(5):563–570, 1980.

[8] N. Ashwear, G. Tamadapu, and A. Eriksson. Optimization of modular tensegrity structures for high stiffness and frequency separation requirements. *International Journal of Solids and Structures*, 80:297–309, 2016.

[9] J. Barta. On the minimum weight of certain redundant structures. *Acta Tech Acad Sci Hung*, 18:67–76, 1957.

[10] M.P. Bendsøe and A.R. Diaz. A method for treating damage related criteria in optimal topology design of continuum structures. *Structural and Multidisciplinary Optimization*, 16(2-3):108–115, 1998.

[11] M. Bruggi and P. Duysinx. Topology optimization for minimum weight with compliance and stress constraints. *Structural and Multidisciplinary Optimization*, 46(3):369–384, 2012.

[12] G.D. Cheng and X. Guo. ε-relaxed approach in structural topology optimization. *Structural Optimization*, 13(4):258–266, 1997.

[13] K.H. Chew, K. Tai, E.Y.K. Ng, and M. Muskulus. Analytical gradient-based optimization of offshore wind turbine substructures under fatigue and extreme loads. *Marine Structures*, 47:23–41, 2016.

[14] K.K. Choi and N.-H. Kim. *Structural Sensitivity Analysis and Optimization 1*. Springer New York, 2005.

[15] C. Cid, A. Baldomir, and S. Hernández. Probability-damage approach for fail-safe design optimization (PDFSO). *Structural and Multidisciplinary Optimization*, 62:3149–3163, 2020.

[16] R. D. Cook, D. S. Malkus, M. E. Plesha, and R. J. Witt. *Concepts and applications of finite element analysis*. John Wiley & Sons, 4th Edition, 2002.

[17] S. Dou and J.S. Jensen. Optimization of nonlinear structural resonance using the incremental harmonic balance method. *Journal of Sound and Vibration*, 334:239–254, 2015.

[18] S. Dou and M. Stolpe. On stress-constrained fail-safe structural optimization considering partial damage. *Structural and Multidisciplinary Optimization*, 63:929–933, 2021.

[19] J.Z. Du, F.W. Meng, Y.H. Guo, and Y.K. Sui. Fail-safe topology optimization of continuum structures with fundamental frequency constraints based on the ICM method. *Acta Mechanica Sinica/lixue Xuebao*, 36(5):1065–1077, 2020.

[20] P. Duysinx and M.P. Bendsøe. Topology optimization of continuum structures with local stress constraints. *International Journal for Numerical Methods in Engineering*, 43(8):1453–1478, 1998.

[21] R. Fletcher. *Practical Methods of Optimization: Vol. 2: Constrained Optimization.* Wiley, New York, 1981.

[22] B.A. Izzuddin, A.G. Vlassis, A.Y. Elghazouli, and D.A. Nethercot. Progressive collapse of multi-storey buildings due to sudden column loss—Part I: Simplified assessment framework. *Engineering structures*, 30(5):1308–1318, 2008.

[23] M. Jansen, G. Lombaert, M. Schevenels, and O. Sigmund. Topology optimization of fail-safe structures using a simplified local damage model. *Structural and Multidisciplinary Optimization*, 49(4):657–666, 2014.

[24] Y. Kanno. Redundancy optimization of finite-dimensional structures: Concept and derivative-free algorithm. *Journal of Structural Engineering*, 143(1):04016151, 2017.

[25] Y. Kanno and Y. Ben-Haim. Redundancy and robustness, or when is redundancy redundant? *Journal of Structural Engineering*, 137(9):935–945, 2011.

[26] U. Kirsch. Optimal topologies of truss structures. *Computer Methods in Applied Mechanics and Engineering*, 72(1):15–28, 1989.

[27] U. Kirsch. On singular topologies in optimum structural design. *Structural Optimization*, 2(3):133–142, 1990.

[28] K. Long, X. Wang, and Y. Du. Robust topology optimization formulation including local failure and load uncertainty using sequential quadratic programming. *International Journal of Mechanics and Materials in Design*, 15(2):317–332, 2019.

[29] J.K. Lüdeker and B. Kriegesmann. Fail-safe optimization of beam structures. *Journal of Computational Design and Engineering*, 6(3):260–268, 2019.

[30] D.P. Mohr, I. Stein, T. Matzies, and C.A. Knapek. Redundant robust topology optimization of truss. *Optimization and Engineering*, 15(4):945–972, 2014.

[31] M. Muskulus and S. Schafhirt. Design optimization of wind turbine support structures-a review. *Journal of Ocean and Wind Energy*, 1(1):12–22, 2014.

[32] J. Oest, K. Sandal, S. Schafhirt, L.E. Stieng, and M. Muskulus. On gradient-based optimization of jacket structures for offshore wind turbines. *Wind Energy*, 21(11):953–967, 2018.

[33] X. Peng and Y. Sui. Lightweight topology optimization with consideration of the fail-safe design principle for continuum structures. *Engineering Optimization*, 53:32–48, 2021.

[34] N. Pollini. Fail-safe optimization of viscous dampers for seismic retrofitting. *Earthquake Engineering & Structural Dynamics*, 49(15):1599–1618, 2020.

[35] G.I.N. Rozvany. Difficulties in truss topology optimization with stress, local buckling and system stability constraints. *Structural Optimization*, 11:213–217, 1996.

[36] G.I.N. Rozvany. On design-dependent constraints and topologies. *Structural and Multidisciplinary Optimization*, 21:164–172, 2001.

[37] K. Sandal, A. Verbart, and M. Stolpe. Conceptual jacket design by structural optimization. *Wind Energy*, 21(12):1423–1434, 2018.

[38] M.A. Save. Remarks on minimum-volume designs of a three-bar truss. *Journal of Structural Mechanics*, 11(1):101–110, 1983.

[39] A. Serafinska, K. Özenç, and M. Kaliske. A coupled approach of optimization, uncertainty analysis and configurational mechanics for a fail-safe design of structures. *International Journal for Numerical Methods in Engineering*, 109(1):125–152, 2017.

[40] H.A. Smith and J.A. Norato. Topology optimization of fail-safe structures via geometry projection. In *AIAA Scitech 2021 Forum*. AIAA, 2021.

[41] M. Stolpe. Fail-safe truss topology optimization. *Structural and Multidisciplinary Optimization*, 60(4):1605–1618, 2019.

[42] L.L. Stromberg, A. Beghini, W.F. Baker, and G.H. Paulino. Application of layout and topology optimization using pattern gradation for the conceptual design of buildings. *Structural and Multidisciplinary Optimization*, 43(2):165–180, 2011.

[43] L.L. Stromberg, A. Beghini, W.F. Baker, and G.H. Paulino. Topology optimization for braced frames: combining continuum and beam/column elements. *Engineering Structures*, 37:106–124, 2012.

[44] P.F. Sun, J.S. Arora, and E.J. Haug. Fail-safe optimal design of structures. *Engineering Optimization*, 2(1):43–53, 1976.

[45] G. Sved. The minimum weight of certain redundant structures. *Aust J Appl Sci*, 5:1–9, 1954.

[46] G. Sved and Z. Ginos. Structural optimization under multiple loading. *International Journal of Mechanical Sciences*, 10(10):803–805, 1968.

[47] The Mathworks, Inc. *MATLAB R2019a*. Natick, Massachusetts, 2019.

[48] A. Verbart and M. Stolpe. A working-set approach for sizing optimization of frame-structures subjected to time-dependent constraints. *Structural and Multidisciplinary Optimization*, 58(4):1367–1382, 2018.

[49] A.G. Vlassis, B.A. Izzuddin, A.Y. Elghazouli, and D.A. Nethercot. Progressive collapse of multi-storey buildings due to sudden column loss—Part II: Application. *Engineering Structures*, 30(5):1424–1438, 2008.

[50] H. Wang, J. Liu, G. Wen, and Y.M. Xie. The robust fail-safe topological designs based on the von mises stress. *Finite Elements in Analysis and Design*, 171:103376, 2020.

[51] M. Zhou and R. Fleury. Fail-safe topology optimization. *Structural and Multidisciplinary Optimization*, 54(5):1225–1243, 2016.

[52] Z.H. Zuo, Y.M. Xie, and X. Huang. Evolutionary topology optimization of structures with multiple displacement and frequency constraints. *Advances in Structural Engineering*, 15(2):359–372, 2012.